Eur. Phys. J. C (2025) 85:86
https://doi.org/10.1140/epjc/s10052-024-13531-w

THE EUROPEAN PHYSICAL JOURNAL C

Regular Article - Experimental Physics

Measurement of the production cross section of prompt Ξ_c^0 baryons in p–Pb collisions at $\sqrt{s_{NN}} = 5.02$ TeV

ALICE Collaboration[⋆]

CERN, 1211, Geneva 23, Switzerland

Received: 16 June 2024 / Accepted: 21 October 2024

Abstract The transverse momentum (p_T) differential production cross section of the promptly produced charm-strange baryon Ξ_c^0 (and its charge conjugate $\overline{\Xi_c^0}$) is measured at midrapidity via its hadronic decay into $\pi^+\Xi^-$ in p–Pb collisions at a centre-of-mass energy per nucleon–nucleon collision $\sqrt{s_{NN}} = 5.02$ TeV with the ALICE detector at the LHC. The Ξ_c^0 nuclear modification factor (R_{pPb}), calculated from the cross sections in pp and p–Pb collisions, is presented and compared with the R_{pPb} of Λ_c^+ baryons. The ratios between the p_T-differential production cross section of Ξ_c^0 baryons and those of D^0 mesons and Λ_c^+ baryons are also reported and compared with results at forward and backward rapidity from the LHCb Collaboration. The measurements of the production cross section of prompt Ξ_c^0 baryons are compared with a model based on perturbative QCD calculations of charm-quark production cross sections, which includes only cold nuclear matter effects in p–Pb collisions, and underestimates the measurement by a factor of about 50. This discrepancy is reduced when the data is compared with a model that includes string formation beyond leading-colour approximation or in which hadronisation is implemented via quark coalescence. The p_T-integrated cross section of prompt Ξ_c^0-baryon production at midrapidity extrapolated down to $p_T = 0$ is also reported. These measurements offer insights and constraints for theoretical calculations of the hadronisation process. Additionally, they provide inputs for the calculation of the charm production cross section in p–Pb collisions at midrapidity.

1 Introduction

Measurements of heavy-flavour hadron production in hadronic collisions provide crucial tests for calculations based on quantum chromodynamics (QCD). Calculations of p_T-differential heavy-flavour hadron production cross sections in hadronic collisions are factorised into three separate components: the parton distribution functions (PDFs), which describe the Bjorken-x distributions of quarks and gluons within the incoming hadrons for a given transferred momentum squared Q^2; the hard-scattering cross section for the partons to produce a charm- or beauty-quark pair; and the fragmentation functions, which characterise the hadronisation of a quark to a given hadron species [1]. The hadronisation process is typically described via two different mechanisms: fragmentation and recombination (also known as coalescence). In the former, colour neutrality is reached by means of gluon radiation and gluon splitting into quark pairs, with a final phase in which quark pairs or triplets bind together to form mesons or baryons. In the latter, two or three quarks close in the velocity and coordinate space, bind to form color-neutral hadrons. As charm and beauty quarks have masses much larger than Λ_{QCD}, which is the energy scale in QCD at which quarks and gluons are confined within hadrons, the parton–parton hard-scattering cross sections can be calculated perturbatively [2]. In contrast, the fragmentation functions cannot be calculated with perturbative QCD (pQCD) methods, so they are determined from measurements in e^+e^- collisions. They are then applied in cross section calculations, assuming that the relevant hadronisation processes are "universal", i.e. independent of the collision energy and system. A recent review with a more comprehensive overview of heavy-quark hadronisation can be found in Ref. [3]. Factorisation can be implemented in pQCD-based calculations in different ways, for example, in terms of the transferred momentum squared (collinear factorisation) [1]. Calculations for LHC energies, like the general-mass variable-flavour-number scheme (GM-VFNS) [4,5] and the fixed order plus next-to-leading logarithms (FONLL) approach [6,7] provide a next-to-leading order (NLO) accuracy with all-order resummation of next-to-leading logarithms. These calculations describe the production of heavy-flavour mesons within uncertainties in wide kinematic and pp collision-energy ranges [8–11]. The dominant source of theoretical uncertainty in these calculations is related to the choice of the energy scales for the valid-

⋆ e-mail: alice-publications@cem.ch

Published online: 27 January 2025

ity of the perturbative regime (factorisation and renormalisation scales). Charm-hadron production cross sections are also compared with the POWHEG pQCD calculations of charm-quark production with NLO accuracy [12], matched with PYTHIA 6 [13] to generate the parton shower and fragmentation. The POWHEG+PYTHIA 6 simulations describe the charm-meson production cross sections but largely underpredict the production of charm baryons [14]. To isolate the effects of hadronisation, hadron-to-hadron production ratios within the charm sector, such as $\mathrm{D_s^+/D^0}$, $\Lambda_c^+/\mathrm{D^0}$, and $\Xi_c^0/\mathrm{D^0}$ are particularly effective, since in pQCD calculations the PDFs and the choice of the factorisation and renormalisation scales are common to all charm-hadron species and their effects almost fully cancel in the yield ratios.

Previous measurements of charm-meson production cross sections in pp and p–Pb collisions at the LHC [9,10,15–19] show that the $\mathrm{D^+/D^0}$ ratio is independent of the transverse momentum within uncertainties, while a hint of increase with p_{T} is visible for the $\mathrm{D_s^+/D^0}$, $\mathrm{D_s^+/D^+}$, and $\mathrm{D_s^+/(D^0 + D^+)}$ ratios in the interval $p_{\mathrm{T}} < 8$ GeV/c. The ratios are also described well by pQCD calculations and by the PYTHIA 8 event generator using the Monash tune [20,21], with the fragmentation tuned on $\mathrm{e^+e^-}$ collisions. However, the charm baryon-to-meson ratios $\Lambda_c^+/\mathrm{D^0}$, $\Xi_c^{0,+}/\mathrm{D^0}$, $\Omega_c^0/\mathrm{D^0}$, and $\Sigma_c^{0,++}/\mathrm{D^0}$ measured at midrapidity at the LHC [14,22–30] show significant deviations from the values measured in $\mathrm{e^+e^-}$ collisions, and the Monash tune of PYTHIA 8 significantly underpredicts the production rates of charm baryons. These results pose a challenge to the assumption of a universal hadronisation mechanism [31]. Models that incorporate other effects such as string formation beyond the leading-colour approximation [32,33], coalescence or recombination of charm quarks with quarks or di-quarks from a thermal medium [34–36], and statistical hadronisation including higher charm-resonant states not yet discovered [37] provide a better description of the data. Measurements of beauty-baryon production in pp and p–Pb collisions by the CMS, LHCb, and ALICE Collaborations [38–43] also indicate similar differences in hadronisation mechanisms in the beauty sector between hadronic and leptonic collision systems [31–33]. The enhancement of the relative abundance of baryons compared to that of mesons has a strong impact on the charm-quark fragmentation fractions, as demonstrated in pp collisions at $\sqrt{s} = 5.02$ TeV and $\sqrt{s} = 13$ TeV [18,44].

Measurements in proton–nucleus collisions allow an assessment of the various effects, denoted as cold-nuclear-matter (CNM) effects, related to the presence of one or more nuclei in the colliding system. In the initial state, the PDFs are modified in bound nucleons compared to free nucleons, depending on x and Q^2 [45,46]. At LHC energies, the most relevant effect is shadowing: a reduction of the parton densities at low x, which intensifies when Q^2 decreases and the nucleus mass number A increases. This effect, induced by the high phase-space density of small-x partons, can be described within the collinear factorisation framework using phenomenological parametrisations of the modification of the PDFs (denoted as nPDFs) [47–49]. If the parton phase-space reaches saturation, PDF evolution equations are not applicable, and the most appropriate theoretical description is the Colour Glass Condensate effective theory (CGC) [50]. The modification of the small-x parton dynamics can significantly reduce charm-hadron production at low p_{T}. Furthermore, the multiple scattering of partons in the nucleus before and/or after the hard scattering can modify the kinematic distribution of the produced hadrons: partons can lose energy in the initial stages of the collision via initial-state radiation [51], or experience transverse momentum broadening due to multiple soft collisions before the heavy-quark pair is produced [52,53]. These initial-state effects are expected to have a small impact on charm-hadron production at high p_{T} ($p_{\mathrm{T}} >$ 3–4 GeV/c), but they can induce a significant modification of the yield and momentum distribution in the lower p_{T} region.

The nuclear modification factor R_{pPb} (the ratio of the cross section in p–Pb collisions to that in pp interactions scaled by the mass number of the Pb nucleus) of D mesons measured by ALICE in p–Pb collisions at a centre-of-mass energy per nucleon–nucleon collision $\sqrt{s_{\mathrm{NN}}} = 5.02$ TeV is consistent with unity for $0 < p_{\mathrm{T}} < 36$ GeV/c [54], suggesting that the cold-nuclear-matter effects that influence charm-meson production at midrapidity are small. However, measurements of Λ_c^+ baryons in p–Pb collisions [23] indicate a p_{T}-dependent R_{pPb}, with values lower than unity for $0 < p_{\mathrm{T}} < 2$ GeV/c and systematically above unity for $p_{\mathrm{T}} > 2$ GeV/c, indicating an increase in the Λ_c^+ mean p_{T} in p–Pb collisions with respect to pp collisions. A POWHEG+PYTHIA 6 simulation, which is coupled with the EPPS16 nPDF set [55] for p-Pb collisions, is in fair agreement with the Λ_c^+ measurements for $p_{\mathrm{T}} < 3$ GeV/c, but it does not describe the R_{pPb} increase above unity in the region $4 < p_{\mathrm{T}} < 8$ GeV/c. Measurements in the light-flavour sector in high-multiplicity pp and p–Pb collisions at different energies have revealed strong long-range correlations [8], resembling those measured in Pb–Pb collisions, the latter being understood as due to a collective flow related to the formation of a deconfined QCD medium, the quark–gluon plasma. A modification of the p_{T} shape as a function of multiplicity is observed in the strangeness sector by the ALICE and CMS Collaborations in p–Pb collisions [56,57] and is consistent with the effect of radial flow in hydrodynamic models such as EPOS LHC [58]. In this picture, particles of larger mass are boosted to higher transverse momenta by a common velocity field [59]. In the heavy-flavour sector, differential studies of Λ_c^+ and $\mathrm{D^0}$ production as a function of charged-particle multiplicity in pp collisions at $\sqrt{s} = 13$ TeV by ALICE [60] revealed a multiplicity dependence of baryon-to-meson yield ratios. In addition, baryon

production at intermediate p_{T} may be enhanced due to hadronisation via quark recombination [34,36,61]. This can be further examined by measuring the Ξ_{c}^{0}-baryon production in p–Pb collisions and comparing it with the results published in pp collisions [26,27].

In this paper, the measurement of the p_{T}-differential production cross section of prompt Ξ_{c}^{0} baryons in the region $2 < p_{\mathrm{T}} < 12$ GeV/c in p–Pb collisions at $\sqrt{s_{\mathrm{NN}}} = 5.02$ TeV is reported. The term *prompt* refers to charm-hadrons produced directly in the hadronisation of a charm quark or the strong decay of a directly produced excited charm-hadron state, in contrast to *feed-down* charm-hadrons, produced in the decay of a hadron containing a beauty quark. To gauge possible modifications of the p_{T} distribution of promptly produced Ξ_{c}^{0} baryons due to the presence of nuclei in the collision system, the nuclear modification factor is also evaluated. Furthermore, information on the hadronisation process can be extracted by comparing the production cross sections of different hadron species. The p_{T}-dependent yield ratios of $\Xi_{\mathrm{c}}^{0}/\mathrm{D}^{0}$ and $\Xi_{\mathrm{c}}^{0}/\Lambda_{\mathrm{c}}^{+}$ are reported in this article. Finally, by integrating the p_{T}-differential results and extrapolating them to $p_{\mathrm{T}} = 0$, the p_{T}-integrated prompt Ξ_{c}^{0} production cross section is computed. This allows the calculation of the charm fragmentation fractions and of the total charm cross section in p–Pb collisions, reported in Ref. [62].

2 Experimental setup and data samples

The ALICE detector system and its performance are described in detail in Refs. [63,64]. The reconstruction of charm baryons from their hadronic decay products at midrapidity primarily relies on the inner tracking system (ITS) [65] for the reconstruction of charged-particle trajectories and determination of primary and decay vertices, the time projection chamber (TPC) [66] for track reconstruction and particle identification (PID) through specific energy loss measurements, and the time-of-flight detector (TOF) [67], which extends the PID capabilities of the TPC by measuring the flight time of the charged particles from the interaction point. These detectors are located inside a solenoidal magnet of field strength 0.5 T directed along the beam axis. In addition, the two V0 scintillator arrays [68] are used to trigger collision events and determine the luminosity when used in conjunction with the T0 detector [69]. The zero-degree calorimeter (ZDC) is employed for offline event selection in p–Pb collisions [64].

The analysis was performed in the pseudorapidity interval $|\eta| < 0.8$ on data from p–Pb collisions at $\sqrt{s_{\mathrm{NN}}} = 5.02$ TeV collected with a minimum-bias (MB) trigger during Run 2 of the LHC. For p–Pb collisions, the rapidity in the nucleon–nucleon centre-of-mass system (y_{cms}) is shifted by 0.46 units in the direction of the proton beam due to the energy asymmetry of the colliding beams. The results are reported for the rapidity interval $|y_{\mathrm{lab}}| < 0.5$ in the laboratory system, which corresponds to $-0.96 < y_{\mathrm{cms}} < 0.04$.

The MB trigger requires a pair of coincident signals in the two V0 scintillator arrays, which are located on each side of the interaction point. Further offline selections were applied to suppress the background originating from beam–gas collisions and other machine-related background sources [70]. In order to maintain uniform ITS acceptance in pseudorapidity, only events with a reconstructed vertex position within 10 cm along the beam axis from the nominal interaction point were analysed. The primary vertex position was determined using tracks reconstructed in the TPC and ITS detectors. Events with multiple interaction vertices reconstructed from TPC and ITS tracks were tagged as pileup from several collisions and removed from the analysed sample [64]. Using these selection criteria, the p–Pb sample comprised approximately 600 million events, corresponding to an integrated luminosity of $\mathscr{L}_{\mathrm{int}} = 287 \pm 11\ \mu\mathrm{b}^{-1}$.

3 Data analysis

In this analysis, Ξ_{c}^{0} baryons were reconstructed via the decay channel $\Xi_{\mathrm{c}}^{0} \rightarrow \pi^{+}\Xi^{-}$ and its charge conjugate, with branching ratio BR = (1.43 ± 0.32)% [71]. The Ξ^{-} baryons were selected from the decay chain $\Xi^{-} \rightarrow \pi^{-}\Lambda$, BR = (99.887 ± 0.035)%, followed by $\Lambda \rightarrow \pi^{-}\mathrm{p}$, BR = (63.9 ± 0.5)% [71]. The Ξ^{-} and Λ baryons were reconstructed by exploiting their characteristic decay topologies as reported in Refs. [72,73]. Charged-particle tracks and particle-decay vertices were reconstructed using the ITS and the TPC. The particle trajectories in the vicinity of the primary vertex and the decay vertices were reconstructed with the KFParticle package [74], which allows a direct estimate of their parameters and the associated uncertainties. The package allows one to set constraints on the mass and the production point of the reconstructed particles, using information about the uncertainties of the decay-product trajectories to improve the reconstruction accuracy of the parent particle. The mass constraint improves the mass and momentum reconstruction of the particle, while the production point constraint helps to determine whether the particle is coming from a given vertex. These constraints were applied to the Λ and Ξ^{-} decay vertices in the Ξ_{c}^{0} decay chain reconstruction.

Several selection criteria were applied for the initial filtering of Ξ_{c}^{0} candidates. To ensure good quality of the tracks used to reconstruct the Ξ_{c}^{0} candidates, track quality and kinematic selection criteria were applied. The tracks were required to be within the pseudorapidity interval $|\eta| < 0.8$ and to have crossed at least 70 TPC pad rows out of a maximum of 159. The number of clusters in the TPC used for the energy loss determination was required to be larger than

50 to enhance the precision of the mean specific energy loss ($\mathrm{d}E/\mathrm{d}x$) measurement. Moreover, the candidate tracks of the π^+ produced in the Ξ_c^0 decay were required to have a minimum of three (out of six) hits in the ITS.

The PID selections were based on the difference between the measured and expected detector signals for a given particle species hypothesis in units of the detector resolution (n_σ^{det}). For candidate tracks of the pions from the Λ and Ξ^- decays and of the proton from the Λ decay, a selection on the measured $\mathrm{d}E/\mathrm{d}x$ in the TPC of $|n_\sigma^{\mathrm{TPC}}| < 4$ was applied. For the pion from the Ξ^- decay, the transverse momentum was required to be larger than 150 MeV/c, and, if the track has an associated hit in the TOF detector, a further PID selection of $|n_\sigma^{\mathrm{TOF}}| < 5$ was applied to its flight time. The deviation of the measured invariant masses from the world-average value of the Λ and Ξ^- masses [71] was required to be within 10 MeV/c^2. To further reduce the background in the Ξ_c^0 candidate sample, a selection on the p_{T} of the pion produced in the Ξ_c^0 decay was applied. It was required to be greater than 1.6, 1.2, 1.0, and 1.0 GeV/c in the 2–4, 4–6, 6–8, and 8–12 Ξ_c^0 p_{T} intervals, respectively.

After applying the selections described above, further rejection of background Ξ_c^0 candidates was obtained using a boosted decision tree (BDT) algorithm. The BDT implementation provided by the XGBoost library was used [75,76]. During the training process, the BDT is presented with labelled samples, where the true classifications of signal and background are known. The algorithm is trained to optimise the classification of the two classes based on the differences in the topology, kinematics, and PID information. Once the BDT is trained, it is applied to the data sample where the classifications are unknown. With the machine learning approach, multiple selection criteria are combined into a single response variable representing the algorithm's confidence in classifying a candidate as a true Ξ_c^0 baryon. After applying a trained BDT model to the data sample, a selection in the BDT response was applied to reduce the large combinatorial background. Independent BDTs were trained for each p_{T} interval in the analysis. The signal samples for the training were obtained from simulated events using the PYTHIA 8.243 [20] Monte Carlo (MC) generator with the Monash tune [21] embedded into an underlying p–Pb collision generated with HIJING 1.36 [77]. The transport of simulated particles within the detector was performed with the GEANT 3 package [78]. The LHC beam conditions and the conditions of the ALICE detectors in terms of active channels, gain, noise level, and alignment, and their evolution with time during the data taking, were taken into account in the simulations. Each PYTHIA 8 event was required to contain a $\mathrm{c\bar{c}}$ quark pair, with at least one hadronising into a Ξ_c^0 baryon, which is forced to decay via the decay channel of interest. Only prompt Ξ_c^0 signal candidates were selected for the training, while feed-down ones were not used since they have a different decay vertex topology. The background sample was selected from a fraction of real data using the same selection criteria described above, with the additional requirement that the invariant mass of the Ξ_c^0 candidate was within the intervals $2.17 < M < 2.39$ GeV/c^2 or $2.55 < M < 2.77$ GeV/c^2 (sidebands) to ensure that the signal region was excluded.

The training variables in the BDT related to the Ξ^- candidates were (i) the reconstructed invariant mass, (ii) the pointing angle of its momentum to the primary vertex, i.e. the angle between the momentum vector of the reconstructed Ξ^- particle and the vector pointing from the reconstructed primary vertex to the Ξ^- decay vertex, (iii) the decay length normalised by its uncertainty, (iv) a normalised χ^2 value, which is obtained by evaluating whether the momentum vector of the Ξ^- candidate points back to the reconstructed primary vertex, and is provided by the KFParticle package. The training variables describing the pion emerging from the Ξ_c^0 decay were the $n\sigma_\pi^{\mathrm{TOF}}$, the $n\sigma_\pi^{\mathrm{TPC}}$ and the distance of closest approach to the primary vertex. The selection on the BDT response was tuned in each p_{T} interval to maximise the expected statistical significance, which is calculated using (i) an estimated value for the signal extrapolated from the Ξ_c^0 production cross section reported in Ref. [26] using a Lévy-Tsallis fit, multiplied by the reconstruction and selection efficiencies for each BDT selection threshold, (ii) an estimate of the background within the signal region obtained by interpolating a fit to the invariant mass distribution in the sidebands of the Ξ_c^0 signal region.

After applying the BDT selections, the raw Ξ_c^0 yield in each p_{T} interval under study was obtained by fitting the invariant mass distribution of the candidates. Examples of those distributions are shown in Fig. 1 for the p_{T} intervals 2–4 and 6–8 GeV/c. A Gaussian function was used to model the signal peak and an exponential (for $p_{\mathrm{T}} > 4$ GeV/c) or parabolic function (in the $2 < p_{\mathrm{T}} < 4$ GeV/c interval) was used to model the background. Due to the small signal-to-background ratio, the standard deviation of the Gaussian signal function was fixed to the value obtained from simulations to improve the fit stability. A Ξ_c^0 signal, with a statistical significance larger than 3, could be extracted in the four considered p_{T} intervals in the range $2 < p_{\mathrm{T}} < 12$ GeV/c.

4 Corrections

The p_{T}-differential production cross section of prompt Ξ_c^0 baryons per unit of rapidity in the interval $-0.96 < y_{\mathrm{cms}} < 0.04$ was calculated from the raw yields as

$$\frac{\mathrm{d}^2\sigma}{\mathrm{d}y\,\mathrm{d}p_{\mathrm{T}}} = \frac{1}{2}\frac{N_{\mathrm{raw}}^{\Xi_c^0+\overline{\Xi_c^0}}(p_{\mathrm{T}}) \times f_{\mathrm{prompt}}(p_{\mathrm{T}})}{\Delta y_{\mathrm{lab}}\,\Delta p_{\mathrm{T}} \times (\mathrm{Acc}\times\varepsilon)_{\mathrm{prompt}}(p_{\mathrm{T}}) \times \mathrm{BR} \times \mathscr{L}_{\mathrm{int}}}, \quad (1)$$

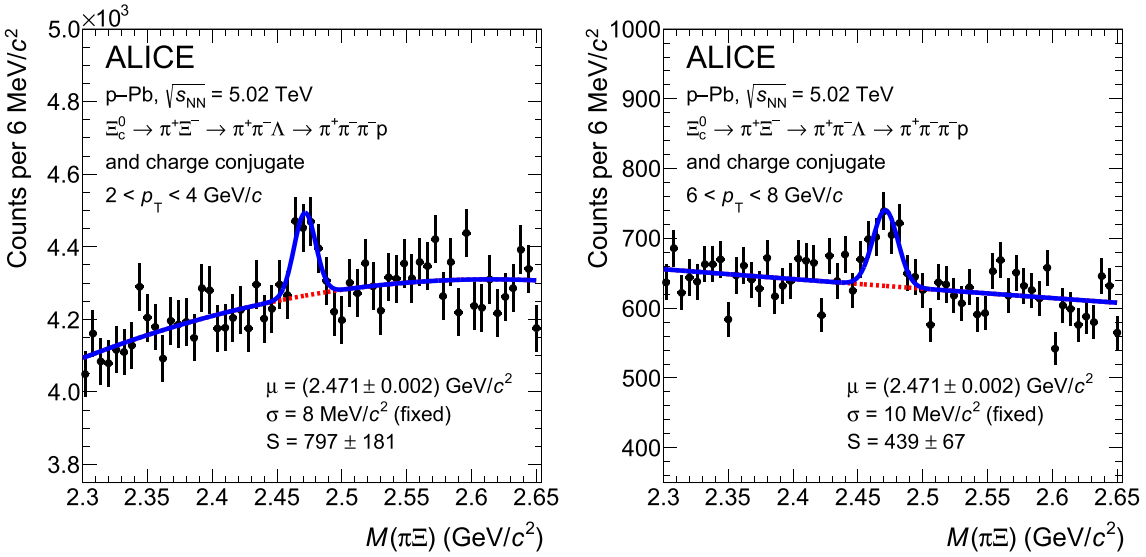

Fig. 1 Invariant mass distributions of $\Xi_c^0 \to \pi^+\Xi^-$ candidates (and charge conjugates) in $2 < p_T < 4$ GeV/c (left), and in $6 < p_T < 8$ GeV/c (right) in p–Pb collisions at $\sqrt{s_{NN}} = 5.02$ TeV. The red dashed curves represent the background fit functions, and the blue curves represent the total fit functions

where $N_{raw}^{\Xi_c^0+\overline{\Xi_c^0}}$ is the raw yield (sum of particles and antiparticles) extracted from the invariant mass fit, f_{prompt} is the fraction of prompt Ξ_c^0 in the measured raw yield, BR is the branching ratio of the considered decay chain, and $\mathscr{L}_{int}$ is the integrated luminosity. The factor 2 accounts for the presence of particles and antiparticles in the raw yields, and $\Delta y_{lab}\,\Delta p_T$ accounts for the widths of the rapidity and transverse momentum intervals. The measurement of Ξ_c^0 is performed for $\Delta y_{lab} = 1.6$, under the assumption that the cross section per unit of rapidity of Ξ_c^0 baryons does not significantly change between $|y_{lab}| < 0.5$ and $|y_{lab}| < 0.8$. This has been verified using PYTHIA 8 simulations [20] and FONLL pQCD calculations [2,6]. The factor $(\text{Acc} \times \varepsilon)_{prompt}$ is the product of the geometrical acceptance (Acc) and the reconstruction and selection efficiency (ε) for prompt Ξ_c^0 candidates and is evaluated using the PYTHIA 8 simulations described in Sect. 3. To account for differences in the p_T-distribution of prompt Ξ_c^0 baryons between the MC simulation and the actual data distribution, weighting factors were applied to the generated Ξ_c^0 p_T-distribution before calculating $(\text{Acc}\times\varepsilon)_{prompt}$. These weighting factors were determined by comparing the p_T-distribution of Ξ_c^0 generated from the Quark Combination Model (QCM) [79] to the PYTHIA 8 distribution described above. The QCM was chosen because it best reproduces the measured Ξ_c^0 p_T distribution. Figure 2 shows the final $(\text{Acc} \times \varepsilon)$ correction factors of prompt and feed-down Ξ_c^0 as a function of p_T. The $(\text{Acc} \times \varepsilon)$ of prompt Ξ_c^0 baryons is slightly larger than that of feed-down baryons. This difference arises from the inclusion of the distance of closest approach (DCA) to the primary vertex of the pion produced in the Ξ_c^0 decay as one of the variables in the BDT training. Since the pions from decays of feed-down Ξ_c^0 present a wider DCA distribution as compared to those from prompt Ξ_c^0, due to the displacement by a few hundred micrometres of the feed-down Ξ_c^0 decay vertices, prompt signals tend to exhibit higher BDT output scores compared to feed-down signals.

The fraction of prompt baryons in the raw Ξ_c^0 yield extracted from the selected candidate sample was calculated as:

$$\begin{aligned} f_{prompt} &= 1 - \frac{N_{feed\text{-}down}^{\Xi_c^0+\overline{\Xi_c^0}}}{N_{raw}^{\Xi_c^0+\overline{\Xi_c^0}}} \\ &= 1 - \frac{1}{N_{raw}^{\Xi_c^0+\overline{\Xi_c^0}}} \frac{\mathrm{d}^2\sigma_{feed\text{-}down}^{\Xi_c^0}}{\mathrm{d}y\,\mathrm{d}p_T} \\ &\quad \times 2 \times (\text{Acc} \times \varepsilon)_{feed\text{-}down} \times R_{pPb,\ feed\text{-}down} \\ &\quad \times \Delta p_T \times \Delta y_{lab} \times \text{BR} \times \mathscr{L}_{int} \end{aligned} \tag{2}$$

The yield of feed-down Ξ_c^0 ($\mathrm{d}^2\sigma_{feed\text{-}down}^{\Xi_c^0}/\mathrm{d}p_T\mathrm{d}y$) is estimated starting from the cross section of Λ_c^+ baryons originating from Λ_b^0 decays, which is obtained using the beauty-quark production cross section from FONLL calculations [6,7], the fraction of beauty quarks fragmenting into beauty hadrons taken from the LHCb measurement of beauty fragmentation fractions in pp collisions at $\sqrt{s} = 13$ TeV [39], and the decay kinematics of beauty hadrons decaying into a final state with a Λ_c^+, which is taken from PYTHIA 8 ($(\mathrm{d}^2\sigma/\mathrm{d}p_T\mathrm{d}y)_{feed\text{-}down,FONLL}^{\Lambda_c^+}$). The predicted feed-down Λ_c^+ cross section is scaled by the ratio of the measured p_T-differential production cross sections of

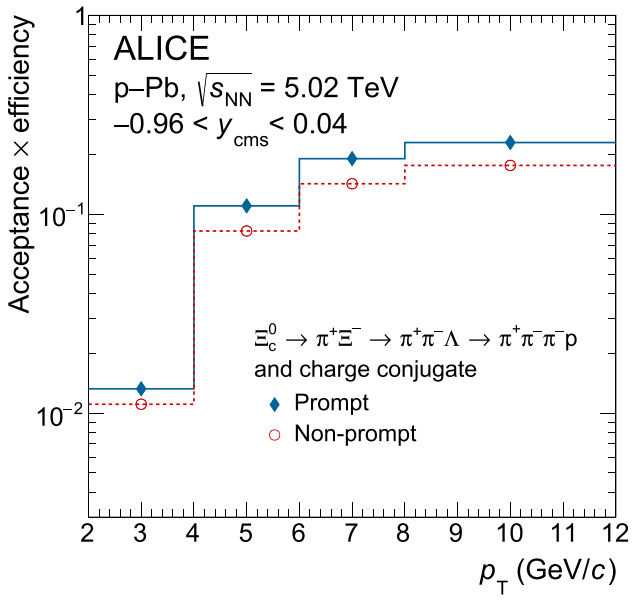

Fig. 2 Product of detector acceptance and efficiency for Ξ_c^0 baryons in p–Pb collisions at $\sqrt{s_{NN}} = 5.02$ TeV as a function of p_T. The solid line corresponds to the (Acc × ε) for prompt Ξ_c^0, while the dotted line represents (Acc × ε) for Ξ_c^0 baryons originating from beauty-hadron decays. The statistical uncertainties are smaller than the marker size

prompt Ξ_c^0 [26] $(d^2\sigma/dp_T dy)^{\Xi_c^0}_{\text{prompt}}$, and prompt Λ_c^+ [24], where the $(d^2\sigma/dp_T dy)^{\Lambda_c^+}_{\text{prompt}}$ was measured in pp collisions at $\sqrt{s} = 5.02$ TeV to obtain an estimation for the p_T-differential feed-down Ξ_c^0 production cross section

$$\frac{d^2\sigma^{\Xi_c^0}_{\text{feed-down}}}{dy\, dp_T} = \left(\frac{d^2\sigma}{dp_T dy}\right)^{\Lambda_c^+}_{\text{feed-down,FONLL}} \times \frac{(d^2\sigma/dp_T dy)^{\Xi_c^0}_{\text{prompt}}}{(d^2\sigma/dp_T dy)^{\Lambda_c^+}_{\text{prompt}}} \quad (3)$$

The scaling factor $(d^2\sigma/dp_T dy)^{\Xi_c^0}_{\text{prompt}}/(d^2\sigma/dp_T dy)^{\Lambda_c^+}_{\text{prompt}}$ approximates the term

$$\frac{\sum_{H_B} b \to H_b \to \Xi_c}{\sum_{H_B} b \to H_b \to \Lambda_c} \simeq \frac{b \to \Xi_b \to \Xi_c}{b \to \Lambda_b \to \Lambda_c} \quad (4)$$

considering that the only beauty baryons that contribute to the yield of Ξ_c (Λ_c^+) are Ξ_b (Λ_b^0). This scaling relies on the assumptions that the p_T shapes of the feed-down Λ_c^+ and Ξ_c^0 production cross sections are similar, and the ratio of production cross sections of Ξ_c^0 and Λ_c^+ is similar for prompt and feed-down baryons. Finally, a hypothesis on the value of the nuclear modification factor R_{pPb} of feed-down Ξ_c^0 is needed. It is assumed that the R_{pPb} of prompt Ξ_c^0 is equal to that of prompt Λ_c^+ and that the R_{pPb} of prompt and feed-down Ξ_c^0 are equal. The evaluated prompt fraction ranges between 0.91 and 0.96 depending on the p_T interval.

Table 1 Systematic uncertainties on the prompt Ξ_c^0 production cross section

	p_T interval (GeV/c)			
	[2,4]	[4,6]	[6,8]	[8,12]
Tracking efficiency	4%	2%	3%	3%
Matching efficiency	1%	1%	1%	1%
BDT selection efficiency	6%	10%	5%	3%
MC p_T shape	5%	1%	1%	1%
Feed-down subtraction	$^{+5}_{-6}$%	$^{+8}_{-11}$%	$^{+10}_{-15}$%	$^{+6}_{-9}$%
Branching ratio	22%			
Luminosity	3.7%			

5 Systematic uncertainties

The contributions to the systematic uncertainty on the prompt Ξ_c^0 production cross section are summarised in Table 1.

The systematic uncertainty on the raw yield extraction was evaluated by repeating the fit to the invariant mass distributions varying: (i) the function used to describe the background, (ii) the minimum and maximum of the invariant mass intervals considered for the fit, and (iii) the Gaussian width of the mass peak by ±10% compared to the value obtained from simulations. The systematic uncertainty was assigned by adding in quadrature the root mean square error (RMS) of the resulting distribution of the raw yield values and the shift of the mean of the distribution with respect to the value obtained with the default fit configuration.

The systematic uncertainty on the track reconstruction efficiency was estimated by (i) varying the track selection criteria in the TPC and (ii) comparing the ITS-TPC matching efficiency in data and simulations. These contributions are reported as "Tracking efficiency" and "Matching efficiency" in Table 1, respectively. The first contribution to the tracking systematic uncertainty was defined as the RMS of the Ξ_c^0 cross section values obtained by repeating the analysis with different TPC track selection criteria. The matching efficiency affects only the pion from the Ξ_c^0 decay since no ITS condition was imposed for tracks coming from the Ξ^- and Λ decays. The per-track uncertainty on the matching efficiency is p_T dependent, and it was propagated to the Ξ_c^0 taking into account the decay kinematics.

The systematic uncertainty on the Ξ_c^0 selection efficiency arises due to possible differences between the real detector resolutions and alignment, and their description in the simulation. This uncertainty was assessed by comparing the production cross sections obtained using different selection criteria. In particular, the selections on the BDT outputs were varied in a range corresponding to a modification of about 40% in the efficiency for the prompt Ξ_c^0. The systematic uncertainty was assigned as the RMS of the resulting pro-

duction cross section distribution. An additional source of systematic uncertainty was assigned due to the dependence of the efficiencies on the generated p_{T} distribution of Ξ_{c}^{0} in the simulation ("MC p_{T} shape" in Table 1). To estimate this effect, the efficiencies were evaluated modifying the weights to match the p_{T} spectrum obtained from PYTHIA 8 simulations using a tune with colour-reconnection topologies beyond the leading-colour approximation [32], which includes so-called "junctions" that fragment into baryons and lead to an increased baryon production with respect to the Monash tune. An uncertainty was assigned in each p_{T} interval based on the difference between the central and the varied efficiency.

The systematic uncertainty on the subtraction of feed-down from beauty-hadron decays was estimated by varying: (i) the factorisation and renormalisation scales, and the beauty quark mass in the FONLL calculations (according to the prescriptions in Ref. [80]), and the hypothesis on the fragmentation functions within the uncertainties of the LHCb measurement (taken from Ref. [81]), (ii) the $\Xi_{\mathrm{c}}^{0}/\Lambda_{\mathrm{c}}^{+}$ ratio, scaling it up by a factor of 2 and down by a factor tuned to accommodate the $\Xi_{\mathrm{b}}^{-}/\Lambda_{\mathrm{b}}^{0}$ ratio measured by the LHCb Collaboration [39], (iii) the hypothesis on the R_{pPb} of feed-down Ξ_{c}^{0} in the range $0.9 < R_{\mathrm{pPb,feed-down}}/R_{\mathrm{pPb,prompt}} < 2$. This range is chosen to cover the uncertainties of the measured Λ_{c}^{+} R_{pPb}. The theoretical calculation from QCM was also considered for the systematic variation of the R_{pPb}.

The uncertainty on the luminosity measurement is 3.7% for p–Pb collisions [82] and the uncertainty on the decay chain branching ratio is 22% [71].

6 Results

The p_{T}-differential cross section of prompt Ξ_{c}^{0}-baryon production in p–Pb collisions at $\sqrt{s_{\mathrm{NN}}} = 5.02$ TeV measured in the transverse momentum interval $2 < p_{\mathrm{T}} < 12$ GeV/c and in the rapidity interval $-0.96 < y_{\mathrm{cms}} < 0.04$ is shown in Fig. 3. In the left panel of Fig. 3, the measured cross section is compared with POWHEG+PYTHIA 6 calculations and with QCM predictions [79].

In POWHEG+PYTHIA 6 calculations, the CT14NLO parton distribution functions [83] are used for the proton, while for the Pb nucleus the nuclear modification of the PDFs is modelled with the EPPS16 nPDF parameterisation [55]. The factorisation and renormalisation scales, μ_{F} and μ_{R}, were taken to be equal to the transverse mass of the quark, $\mu_0 = \sqrt{m^2 + p_{\mathrm{T}}^2}$, and the charm-quark mass was set to $m_{\mathrm{c}} = 1.5$ GeV/c^2. The theoretical uncertainties were estimated by varying these scales in the intervals $0.5\mu_0 < \mu_{\mathrm{F,R}} < 2\mu_0$, with $0.5\mu_0 < \mu_{\mathrm{R}}/\mu_{\mathrm{F}} < 2\mu_0$ based on the prescriptions of Ref. [6]. The uncertainties on the nPDF were not included in the calculation as they are considerably smaller than the scale uncertainties. The POWHEG+PYTHIA 6 calculations underestimate the measurement by about a factor of 50. This discrepancy is mostly attributed to the description of the hadronisation process in PYTHIA 6, which is tuned on $\mathrm{e^+e^-}$ collisions and underestimates baryon production. This is also supported by the $\Xi_{\mathrm{c}}^{0}/\mathrm{D}^{0}$ and $\Xi_{\mathrm{c}}^{0}/\Lambda_{\mathrm{c}}^{+}$ ratios described in the following. Notably, a large difference between the measured Ξ_{c}^{0} production and the predictions from PYTHIA 8 with the Monash tune, in which the hadronisation is tuned on $\mathrm{e^+e^-}$ collisions, was already observed in pp collisions both for the Ξ_{c}^{0} cross section [26] and the baryon-over-meson ratios [26,27]. In the PYTHIA 8 Angantyr calculations [33] the p–Pb collision is treated as a superposition of multiple nucleon–nucleon collisions. In addition, this model implements the colour-reconnection mechanism beyond leading-colour approximation which includes the formation of junctions that fragment into baryons. The junction formation and fragmentation for the colour dipoles containing heavy quarks has been improved. The rope hadronization model, needed to increase the strange quark production in strings breakups, is not yet implemented and its effect is emulated by increasing the overall relative probability of having strange quarks in string breakups. The PYTHIA 8 Angantyr calculations underestimate the measured Ξ_{c}^{0} production cross section in p–Pb collisions by a factor of about 3. The QCM calculations implement charm-quark hadronisation via a simplified approach to hadronisation by coalescence, developed solely in the momentum space, without considering the coordinate space. The model estimates the p_{T} distributions of quarks from a fit to the measured π, K, and D meson spectra, and assumes that hadronisation occurs exclusively through coalescence at all momenta [35,79]. The charm quark is combined with a co-moving light antiquark or two co-moving quarks to form a charm meson or baryon. A free parameter, $R_{\mathrm{B/M}}^{(\mathrm{c})} = 0.425$, characterises the relative production of single-charm baryons to single-charm mesons and it is tuned to reproduce the $\Lambda_{\mathrm{c}}^{+}/\mathrm{D}^{0}$ ratio measured by ALICE in pp collisions at $\sqrt{s} = 7$ TeV [22]. The relative abundances of the different charm-baryon species are determined by thermal weights from the statistical hadronisation approach [84]. The QCM prediction, tuned on the Λ_{c}^{+} production in pp collisions, underestimates the measured Ξ_{c}^{0} production cross section in p–Pb collisions by a factor of about 2. A similar discrepancy was observed in pp collisions [27] when comparing the results to a statistical hadronisation approach [37], which also employs thermal weights to determine the abundances of different charm-baryon species [27].

In the right panel of Fig. 3 the prompt Ξ_{c}^{0}-baryon production cross section measured in p–Pb collisions is compared with the measurement in the semileptonic decay channel in pp collisions at $\sqrt{s} = 5.02$ TeV [26] and with the measure-

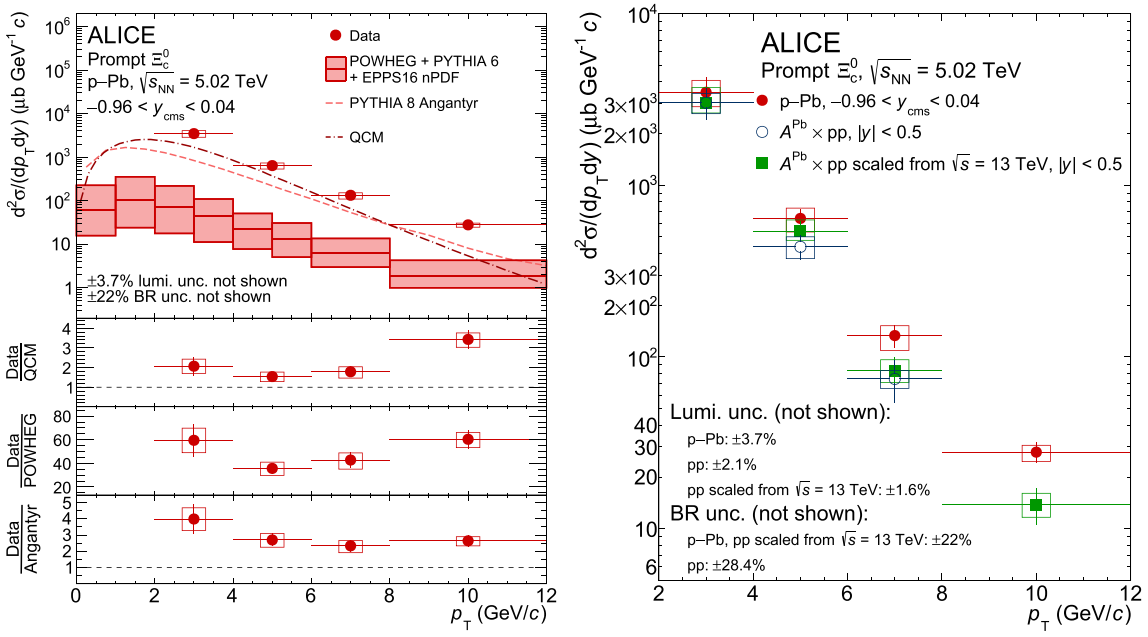

Fig. 3 Prompt Ξ_c^0-baryon p_T-differential cross section in p–Pb collisions at $\sqrt{s_{NN}} = 5.02$ TeV. The statistical uncertainties are shown as vertical bars and the systematic uncertainties are shown as boxes. Left: comparison to predictions from POWHEG+PYTHIA 6 [12,13] simulations matched with the EPPS16 nPDF parameterisation [55], PYTHIA 8 Angantyr calculations [33], and the QCM [79]. The uncertainties on the POWHEG calculation are due to the choice of the pQCD scales and the charm quark mass as described in the text. Right: Comparison with the cross section measured in the semileptonic decay channel in pp collisions at $\sqrt{s} = 5.02$ TeV [26] and in the hadronic decay channel in pp collisions at $\sqrt{s} = 13$ TeV [27] scaled to $\sqrt{s} = 5.02$ TeV (the energy-scaling factor is described in the text). Both the pp measurements are scaled by the atomic mass number A of the Pb nucleus

ment in the hadronic decay channel $\Xi_c^0 \to \pi^+\Xi^-$ in pp collisions at $\sqrt{s} = 13$ TeV [27] scaled to $\sqrt{s} = 5.02$ TeV. Both the pp cross sections are scaled by the atomic mass number $A = 208$ of the lead nucleus. The prompt Ξ_c^0 production cross section measured in pp collisions at $\sqrt{s} = 13$ TeV was first rebinned to match the p_T intervals of the p–Pb measurement. In the rebinning, the raw yield uncertainty was considered uncorrelated across p_T intervals, while all other systematic uncertainties were treated as correlated. The p_T-dependent energy-scaling factor from $\sqrt{s} = 13$ TeV to $\sqrt{s} = 5.02$ TeV was computed as the ratio of D^0-meson production cross section from FONLL calculations in pp collisions at the same collision energies [85]. The ALICE Collaboration has shown that the energy scaling factors for mesons and baryons are compatible within the uncertainties [18]. The uncertainty on the energy-scaling factor was calculated by varying the renormalisation and factorisation scales, the mass of the charm quark, and the nuclear PDFs consistently at the two collision energies. The total uncertainty is calculated as the envelope of the variations. The two results for the Ξ_c^0 cross sections in pp collisions at $\sqrt{s} = 5.02$ TeV are in agreement with each other within uncertainties. The cross section measured via the hadronic decay channel in pp collisions at $\sqrt{s} = 13$ TeV scaled to $\sqrt{s} = 5.02$ TeV is used as the pp reference for the calculation of the nuclear modification factor because the two measurements are performed in the same decay channel and the systematic uncertainty due to the branching ratio, which is the dominant systematic uncertainty, cancels out in the ratio. Furthermore, the cross section in pp collisions at $\sqrt{s} = 13$ TeV was measured in the p_T interval 8–12 GeV/c, allowing the computation of the R_{pPb} up to higher p_T as compared to the measurement in pp collisions at $\sqrt{s} = 5.02$ TeV, which extends only up to $p_T = 8$ GeV/c.

To better investigate any effect due to the collision system, the nuclear modification factor R_{pPb} was calculated as the ratio between the p_T-differential Ξ_c^0 cross section in p–Pb collisions and the reference pp measurement scaled by the nuclear mass number A of the lead nucleus and corrected to account for the rapidity shift between pp and p-Pb collisions using FONLL calculations [6]. The result is shown in Fig. 4. The systematic uncertainties on the branching ratio and beauty feed-down are treated as fully correlated between the two collision systems, and all other systematic uncertainties are considered as uncorrelated. The central values of the Ξ_c^0-baryon R_{pPb} are larger than unity in the full p_T interval of the measurement, even though all data points are compatible with unity within the large uncertainties (the maximal deviation is 1.5σ for the p_T interval 8–12 GeV/c). This also prevents to establish if an increasing trend with p_T is present. The Ξ_c^0 R_{pPb} is compatible with the Λ_c^+ R_{pPb} [14] within

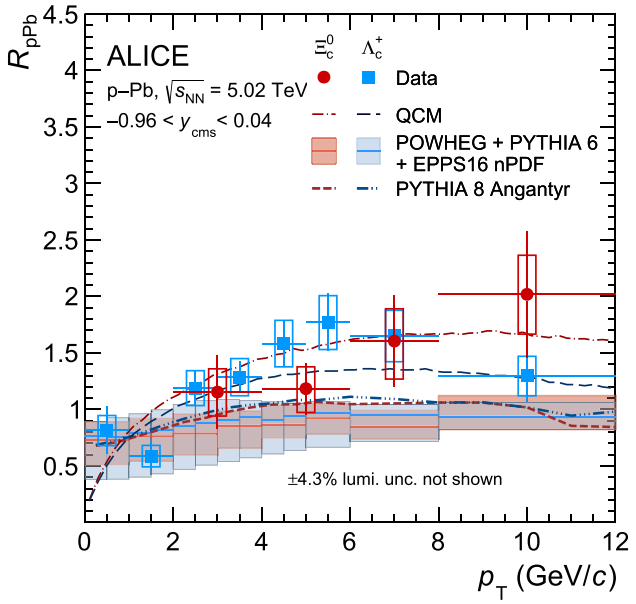

Fig. 4 Nuclear modification factor R_{pPb} of prompt Ξ_c^0 baryons in p–Pb collisions at $\sqrt{s_{NN}} = 5.02$ TeV as a function of p_T compared to the R_{pPb} of Λ_c^+ baryons [14]. The measured R_{pPb} is also compared to POWHEG+PYTHIA 6 with EPPS16 simulations, to PYTHIA 8 Angantyr calculations [33], and to QCM predictions. The statistical uncertainties are shown as vertical bars and the systematic uncertainties are shown as boxes. The uncertainties on the POWHEG calculation are due to the choice of the pQCD scales as described in the text

uncertainties pointing to a similar modification of the production of these two baryon species in p–Pb collisions with respect to pp collisions. The measured R_{pPb} is compared to POWHEG+PYTHIA 6 simulations, PYTHIA 8 Angantyr calculations, and QCM predictions. The only nuclear effect included in the POWHEG + PYTHIA 6 calculations is due to the EPPS16 modification of the PDFs. The resulting R_{pPb} is lower than unity with a mild p_T dependence, and it reproduces within the large uncertainties the measured Ξ_c^0 R_{pPb}. On the other hand, some tension is visible for the Λ_c^+ in the $4 < p_T < 8$ GeV/c interval. The QCM reproduces both measurements within their uncertainties. The comparison with POWHEG+PYTHIA 6 calculations suggests that the deviation of R_{pPb} from unity (significant for the Λ_c^+) may have influences beyond the alteration of the PDFs of nucleons within the nuclei's structure compared to those of protons. Additional effects, possibly related to the hadronisation process and the presence of an expanding medium, may play a role, as suggested by the modification of the Λ_c^+ p_T shape between pp and p–Pb collisions [14]. However, the large uncertainties associated with the Ξ_c^0 results prevent conclusive interpretations, because the measured R_{pPb} exhibits a trend compatible with both the Λ_c^+ and a flat trend. The R_{pPb} obtained from PYTHIA 8 Angantyr calculations shows a mild increasing trend with p_T, reaching unity at $p_T \sim 3$ GeV/c for both Ξ_c^0 and Λ_c^+ and is compatible with the measurements within the large uncertainties.

The ratio of the production cross sections of different hadron species is sensitive to the modification of the hadronisation mechanisms in a partonic environment. The p_T-dependent Ξ_c^0/D^0 baryon-to-meson yield ratio measured in pp and p–Pb collisions at $\sqrt{s_{NN}} = 5.02$ TeV [26] is reported in the left panel of Fig. 5. For the measurement in p–Pb collisions, the prompt D^0 cross section reported in Ref. [54] is used. The systematic uncertainty on the Ξ_c^0/D^0 yield ratio is calculated assuming all the uncertainties of the Ξ_c^0 and D^0 cross sections as uncorrelated, except for the tracking and feed-down systematic uncertainties, which partially cancel in the ratio, and the uncertainty on the luminosity which fully cancels in the ratio. The Ξ_c^0/D^0 ratio in p–Pb collisions hints at a slightly decreasing trend with p_T, similar to the one measured in pp collisions, albeit with large uncertainties. The theoretical predictions from QCM are also shown and they underpredict the Ξ_c^0/D^0 ratios by a similar amount in both collision systems. This discrepancy is predominantly due to the low Ξ_c^0-baryon yield predicted by this model, as it can be seen by the fact that QCM undershoots the Ξ_c^0 cross section (see Fig. 3) and the Ξ_c^0/D^0 yield ratio by the same amount. PYTHIA 8 Angantyr calculations [33] are also shown for both pp and p–Pb collisions. This PYTHIA 8 implementation improves the description for Ξ_c^0 with respect to previous calculations [32] available for pp collisions. However, the model still underestimates the Ξ_c^0/D^0 yield ratio by a similar amount as the QCM model in both pp and p–Pb collisions. One difference between the two models is that the PYTHIA 8 Angantyr calculation does not exhibit a crossing at low p_T between pp and P–Pb collisions, indicating signs of larger radial flow in p–Pb collisions, but the calculation in p–Pb collisions is larger than the pp one in the full p_T interval. POWHEG+PYTHIA 6 calculations predict a slightly increasing trend with p_T, and undershoot the measured Ξ_c^0/D^0 yield ratio by approximately a factor of 20. Given that these predictions underestimate the D^0 production only by a factor of about 2, it is reasonable to conclude that the large discrepancy in the description of the Ξ_c^0-baryon production lies primarily in the hadronisation provided by PYTHIA 6, which is tuned on e^+e^- collisions, rather than in the description of charm production or in an inaccurate modelling of initial state CNM effects. Furthermore, given that a difference of 1.7σ between the Ξ_c^0/D^0 yield ratio in pp and p–Pb collisions is measured in the 6–8 GeV/c p_T interval, it is not possible to conclude on a possible enhancement of this baryon-over-meson yield ratio in p–Pb collisions with respect to pp collisions.

The right panel of Fig. 5 reports the Ξ_c^0/Λ_c^+ baryon-to-baryon yield ratio measured in p–Pb collisions at $\sqrt{s_{NN}} = 5.02$ TeV compared with the ratio measured in pp collisions at $\sqrt{s} = 13$ TeV [27]. The two measurements

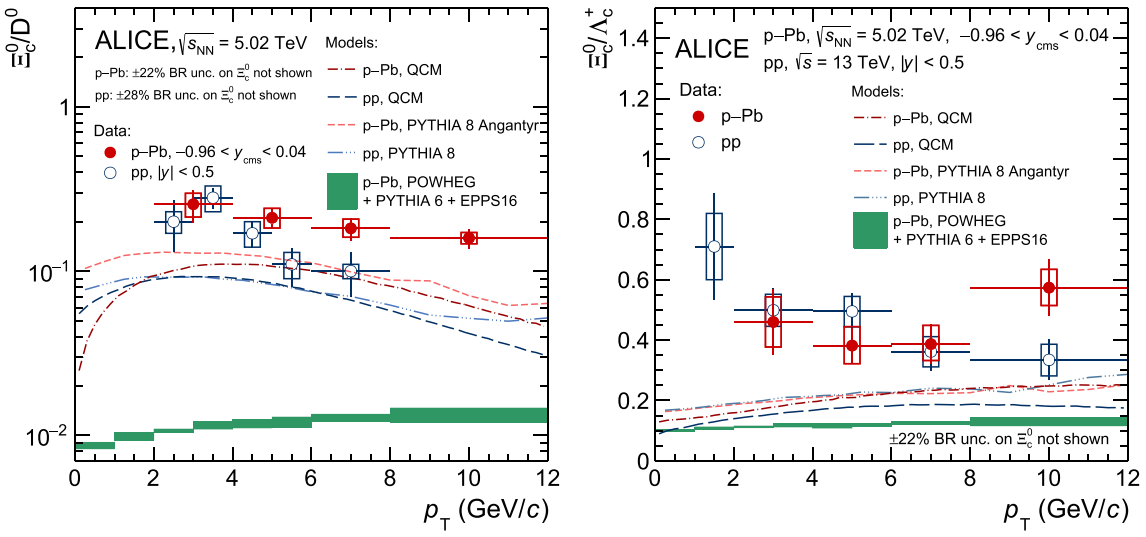

Fig. 5 Left: Ξ_c^0/D^0 ratio as a function of p_T in p–Pb collisions at $\sqrt{s_{NN}} = 5.02$ TeV and in pp collisions at $\sqrt{s} = 5.02$ TeV [26] compared to QCM, POWHEG + PYTHIA 6, and PYTHIA 8 Angantyr predictions. Right: Ξ_c^0/Λ_c^+ ratio as a function of p_T in p–Pb collisions at $\sqrt{s_{NN}} = 5.02$ TeV and in pp collisions at $\sqrt{s} = 13$ TeV [27] compared to QCM, POWHEG + PYTHIA 6, and PYTHIA 8 Angantyr calculations. The BR uncertainties for the Λ_c^+ are evaluated as the weighted average on the two decay channels [22] and are included in the systematic uncertainty box for each p_T bin

are in agreement within uncertainties, and they exhibit no significant p_T dependence within the current measurement uncertainties. This suggests that there is no appreciable additional modification of the hadronisation process when moving from pp to p–Pb collisions. The QCM calculations show a slightly increasing trend as a function of p_T and underestimate the measured ratio by a factor of about 2.5 (1.6) in the 2–4 (6–8) GeV/c p_T intervals. PYTHIA 8 Angantyr calculations in pp and p–Pb collisions are compatible and show a slightly increasing trend as a function of p_T. These calculations underestimate the measured ratio by a factor of about 2.4 (1.7) in the 2–4 (6–8) GeV/c p_T intervals. POWHEG+PYTHIA 6 predictions are also included in the figure, underestimating the Ξ_c^0/Λ_c^+ yield ratio by a factor of about 4 at all p_T. This reflects a similar underprediction in the production of both baryon species. However, the Ξ_c^0-baryon production appears to be underpredicted more than the Λ_c^+-baryon one, suggesting that additional effects, such as recombination, could be considered in order to provide a better description of the results, although the large uncertainties preclude definitive conclusions.

In Fig. 6 the particle ratios measured by ALICE in the central rapidity region ($-0.96 < y_{cms} < 0.04$) in p–Pb collisions at $\sqrt{s_{NN}} = 5.02$ TeV are compared to the Ξ_c^+/D^0 (left panel) and Ξ_c^+/Λ_c^+ (right panel) yield ratios measured by LHCb at forward ($1.5 < y_{cms} < 4.0$) and backward ($-5.0 < y_{cms} < 2.5$) rapidities in p–Pb collisions at $\sqrt{s_{NN}} = 8.16$ TeV [86]. A direct comparison between Ξ_c^0 and Ξ_c^+ results is possible because these two baryons are expected to be produced in equal amounts due to isospin symmetry and it was indeed demonstrated in pp collisions at $\sqrt{s} = 13$ TeV that the production cross sections of these two baryon species are compatible within uncertainties [18]. While the baryon-over-meson yield ratio provides an indication of a rapidity dependence, with the yield ratio at midrapidity being larger than the ones at forward and backward rapidities in the full p_T range (a difference ranging from 1.5σ to 2.0σ is measured across the different p_T intervals), the baryon-over-baryon yield ratios are compatible at mid, forward, and backward rapidity within the uncertainties (a difference of 1.1σ is measured for the 2–4 GeV/c p_T interval). Conducting measurements of baryon-over-meson and baryon-over-baryon yield ratios at the same centre-of-mass energy per nucleon pair for the same hadron reconstructed in the same decay channel will allow the removal of potential ambiguities in the interpretation of the results, helping to unravel possible rapidity dependence of the charm baryon enhancement. PYTHIA 8 Angantyr calculations, computed for p–Pb collisions for different rapidity intervals, are also shown in Fig. 6. A small dependence on the rapidity is observed for the Ξ_c^0/D^0 ratio. The computed ratio is largest at midrapidity and lowest at backward rapidity. This dependence might be introduced by the different parton and string densities in this asymmetric collision system. However, such a difference is not observed for the baryon-to-baryon yield ratio. Although the baryon-to-meson and baryon-to-baryon ratios measured at midrapidity are underestimated by PYTHIA 8 Angantyr, the model agrees with the forward-rapidity measurements within uncertainties.

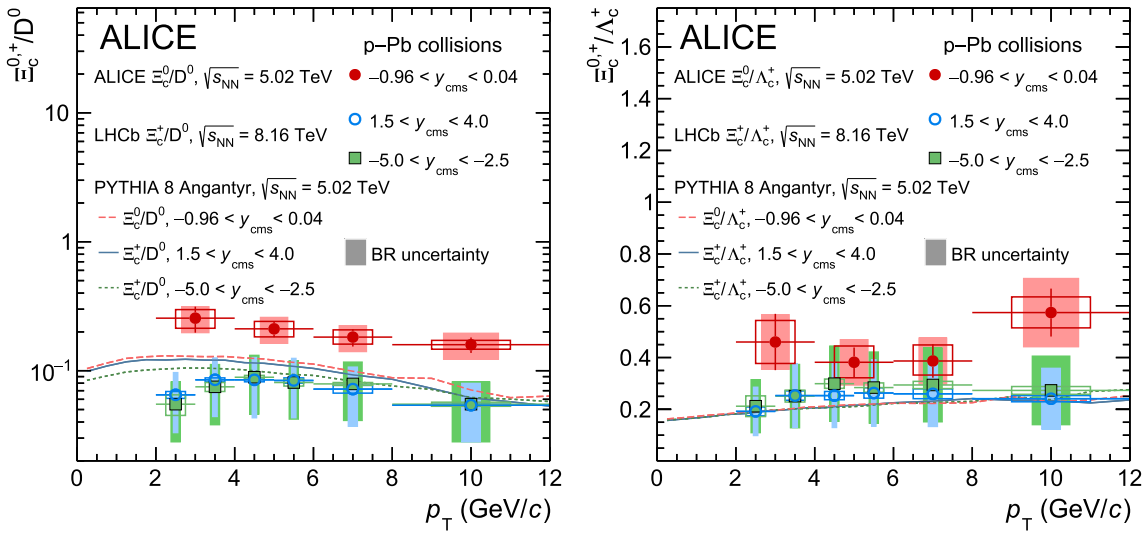

Fig. 6 Ξ_c^0/D^0 (left) and Ξ_c^0/Λ_c^+ (right) ratios as a function of p_T in p–Pb collisions at $\sqrt{s_{NN}} = 5.02$ TeV measured by ALICE, compared to the Ξ_c^+/D^0 and the Ξ_c^+/Λ_c^+ ratio measured by LHCb at $\sqrt{s_{NN}} = 8.16$ TeV [86], and PYTHIA 8 Angantyr predictions [33]

The visible prompt Ξ_c^0-baryon cross section is computed by integrating the p_T-differential cross section in the measured p_T region. In the integration, the systematic uncertainties were propagated considering the uncertainty due to the raw-yield extraction as fully uncorrelated and all the other sources as fully correlated between the p_T intervals. The visible Ξ_c^0-baryon cross section is

$$\mathrm{d}\sigma^{\Xi_c^0}_{\mathrm{pPb}}/\mathrm{d}y\big|^{(2<p_T<12\ \mathrm{GeV}/c)}_{-0.96<y<0.04} = 8.6 \pm 1.6\,(\mathrm{stat.}) \pm 1.3\,(\mathrm{syst.}) \pm 1.9\,(\mathrm{BR}) \pm 0.3\,(\mathrm{lumi.})\ \mathrm{mb}.$$

The p_T-integrated Ξ_c^0 cross section at midrapidity is obtained by extrapolating the visible cross section to the full p_T range. The QCM spectra were chosen to perform the extrapolation, as they provide a reasonable description of the measured p_T shapes for both the production cross section and the Ξ_c^0/D^0 baryon-to-meson yield ratio. The extrapolation factor was calculated as the ratio between the QCM predictions in the full p_T range and those in the p_T interval of the measurement. The scaling factor is 1.74. As QCM does not provide any theory uncertainties, an extrapolation uncertainty was determined using two contributions: (i) the maximum difference among the extrapolation factors obtained with QCM, POWHEG+PYTHIA 6, and PYTHIA 8 Angantyr ($^{+20.6}_{-0.0}$%) and (ii) varying the factorisation and renormalisation scales ($\mu_{F,R}$) and the EPPS16 parameters used in the POWHEG+PYTHIA 6 calculations and determining the maximal relative differences ($^{+23.0}_{-8.6}$%). For the variations of $\mu_{F,R}$, the standard variation ranges were used ($0.5\mu_0 < \mu_{R,F} < 2\mu_0$, with $0.5 < \mu_R/\mu_F < 2$, where $\mu_0 = \sqrt{m_c^2 + p_T^2}$). These contributions were added in quadrature to obtain an overall extrapolation uncertainty of $^{+30.9}_{-8.6}$% on the total Ξ_c^0 production cross section. The resulting p_T integrated cross section for the Ξ_c^0 is

$$\mathrm{d}\sigma^{\Xi_c^0}_{\mathrm{pPb}}/\mathrm{d}y\big|_{-0.96<y<0.04} = 15.0 \pm 2.8\,(\mathrm{stat.})\ ^{+2.2}_{-2.3}\,(\mathrm{syst.}) \pm 3.3\,(\mathrm{BR}) \pm 0.6\,(\mathrm{lumi.})\ ^{+4.6}_{-1.3}\,(\mathrm{extr.})\ \mathrm{mb}.$$

7 Summary

The measurement of prompt Ξ_c^0-baryon production at midrapidity in p–Pb collisions at $\sqrt{s_{NN}} = 5.02$ TeV with the ALICE detector at the LHC is reported. The p_T-differential cross section for the production of prompt Ξ_c^0 baryons is compared to POWHEG+PYTHIA 6 calculations. As seen in pp collisions, the results indicate a significant underestimation, by a factor of about 50, of the Ξ_c^0-baryon yield. This is mainly due to the small fraction of charm quarks hadronising into baryons in the PYTHIA 6 fragmentation stage, which is tuned on results from e^+e^- collisions. PYTHIA 8 Angantyr predictions, with colour reconnections beyond the leading-colour approximation, include the formation of junctions that fragment into baryon. Therefore, the production of Ξ_c^0 baryons is enhanced as compared to POWHEG+PYTHIA 6 calculations and the discrepancy with the measured Ξ_c^0 production cross section is reduced to a factor of about 3. The QCM calculations, which implement charm-quark hadronisation via coalescence and are tuned to reproduce the Λ_c^+/D^0 yield ratio measured by ALICE in pp collisions at $\sqrt{s} = 7$ TeV, provide a better description of the measured Ξ_c^0 production cross section and Ξ_c^0/D^0 yield ratio than POWHEG+PYTHIA 6 calculations, albeit they still underestimate the Ξ_c^0-baryon yield by a factor of about 2. Neither the introduction of

colour reconnections beyond the leading-colour approximation in PYTHIA 8 Angantyr, nor the coalescence mechanism as implemented in QCM quantitatively captures the Ξ_c^0 enhancement relative to the Λ_c^+.

The p_T-differential R_{pPb} is larger than unity in the full p_T interval of the measurement, even though all data points are compatible with unity within the large uncertainties. The R_{pPb} is compatible within uncertainties with both a flat and a slightly increasing trend as the p_T increases, similar to the one observed for Λ_c^+ baryons [14]. It is underpredicted by POWHEG+PYTHIA 6 calculations with the EPPS16 parameterisation of the nuclear PDFs, suggesting that additional final-state effects might be relevant for the Ξ_c^0-baryon production in p–Pb collisions, while the QCM predictions are compatible with the results within the uncertainties. PYTHIA 8 Angantyr predictions provide a similar p_T-differential R_{pPb} for Ξ_c^0 and Λ_c^+ baryons, exhibiting a mild increasing trend with p_T and similar magnitudes to the POWHEG+PYTHIA 6 calculations. The Ξ_c^0 R_{pPb} is compatible with that of Λ_c^+ baryons within uncertainties, possibly hinting to a similar modification of the production of the two baryon species in p–Pb collisions with respect to pp collisions.

The Ξ_c^0/D^0 baryon-to-meson yield ratio shows a slightly decreasing trend with increasing p_T. It is underestimated by the QCM predictions by a factor of about two. This discrepancy originates from the underestimation of the Ξ_c^0 production cross section. The POWHEG+PYTHIA 6 simulations underestimate the measured ratio by a factor of 20, mainly due to the description of the charm-quark fragmentation in PYTHIA 6. The introduction of colour reconnections beyond the leading-colour approximation implemented in PYTHIA 8 Angantyr reduces the data-model discrepancy, but still leads to an underestimation of the Ξ_c^0/D^0 yield ratio similar to that of QCM. The Ξ_c^0/Λ_c^+ ratio is also reported. It is compared to the results obtained in pp collisions at $\sqrt{s} = 13$ TeV. The two measurements are compatible within the uncertainties and do not present a significant p_T dependence. The measured ratios are underestimated by QCM, POWHEG+PYTHIA 6, and PYTHIA 8 Angantyr calculations. The reported Ξ_c^0/D^0 yield ratio is found to be larger than the measurements of Ξ_c^+/D^0 performed by LHCb at forward rapidity, while the Ξ_c^0/Λ_c^+ and Ξ_c^+/Λ_c^+ yield ratios measured in the two rapidity intervals are found to be compatible within uncertainties. Lastly, the p_T-integrated Ξ_c^0 production cross section is measured by extrapolating the visible cross section to the full p_T range using the p_T shape from QCM predictions.

These measurements provide important inputs and constraints to theoretical model calculations of the hadronisation process. Moreover, these results will provide key inputs for the computation of the charm quark fragmentation fractions in p–Pb collisions.

Acknowledgements The ALICE Collaboration would like to thank all its engineers and technicians for their invaluable contributions to the construction of the experiment and the CERN accelerator teams for the outstanding performance of the LHC complex. The ALICE Collaboration gratefully acknowledges the resources and support provided by all Grid centres and the Worldwide LHC Computing Grid (WLCG) collaboration. The ALICE Collaboration acknowledges the following funding agencies for their support in building and running the ALICE detector: A. I. Alikhanyan National Science Laboratory (Yerevan Physics Institute) Foundation (ANSL), State Committee of Science and World Federation of Scientists (WFS), Armenia; Austrian Academy of Sciences, Austrian Science Fund (FWF): [M 2467-N36] and Nationalstiftung für Forschung, Technologie und Entwicklung, Austria; Ministry of Communications and High Technologies, National Nuclear Research Center, Azerbaijan; Conselho Nacional de Desenvolvimento Científico e Tecnológico (CNPq), Financiadora de Estudos e Projetos (Finep), Fundação de Amparo à Pesquisa do Estado de São Paulo (FAPESP) and Universidade Federal do Rio Grande do Sul (UFRGS), Brazil; Bulgarian Ministry of Education and Science, within the National Roadmap for Research Infrastructures 2020-2027 (object CERN), Bulgaria; Ministry of Education of China (MOEC) , Ministry of Science & Technology of China (MSTC) and National Natural Science Foundation of China (NSFC), China; Ministry of Science and Education and Croatian Science Foundation, Croatia; Centro de Aplicaciones Tecnológicas y Desarrollo Nuclear (CEADEN), Cubaenergía, Cuba; Ministry of Education, Youth and Sports of the Czech Republic, Czech Republic; The Danish Council for Independent Research | Natural Sciences, the VILLUM FONDEN and Danish National Research Foundation (DNRF), Denmark; Helsinki Institute of Physics (HIP), Finland; Commissariat à l'Energie Atomique (CEA) and Institut National de Physique Nucléaire et de Physique des Particules (IN2P3) and Centre National de la Recherche Scientifique (CNRS), France; Bundesministerium für Bildung und Forschung (BMBF) and GSI Helmholtzzentrum für Schwerionenforschung GmbH, Germany; General Secretariat for Research and Technology, Ministry of Education, Research and Religions, Greece; National Research, Development and Innovation Office, Hungary; Department of Atomic Energy Government of India (DAE), Department of Science and Technology, Government of India (DST), University Grants Commission, Government of India (UGC) and Council of Scientific and Industrial Research (CSIR), India; National Research and Innovation Agency – BRIN, Indonesia; Istituto Nazionale di Fisica Nucleare (INFN), Italy; Japanese Ministry of Education, Culture, Sports, Science and Technology (MEXT) and Japan Society for the Promotion of Science (JSPS) KAKENHI, Japan; Consejo Nacional de Ciencia (CONACYT) y Tecnología, through Fondo de Cooperación Internacional en Ciencia y Tecnología (FONCICYT) and Dirección General de Asuntos del Personal Academico (DGAPA), Mexico; Nederlandse Organisatie voor Wetenschappelijk Onderzoek (NWO), Netherlands; The Research Council of Norway, Norway; Pontificia Universidad Católica del Perú, Peru; Ministry of Science and Higher Education, National Science Centre and WUT ID-UB, Poland; Korea Institute of Science and Technology Information and National Research Foundation of Korea (NRF), Republic of Korea; Ministry of Education and Scientific Research, Institute of Atomic Physics, Ministry of Research and Innovation and Institute of Atomic Physics and Universitatea Nationala de Stiinta si Tehnologie Politehnica Bucuresti, Romania; Ministry of Education, Science, Research and Sport of the Slovak Republic, Slovakia; National Research Foundation of South Africa, South Africa; Swedish Research Council (VR) and Knut & Alice Wallenberg Foundation (KAW), Sweden; European Organization for Nuclear Research, Switzerland; Suranaree University of Technology (SUT), National Science and Technology Development Agency (NSTDA) and National Science, Research and Innovation Fund (NSRF via PMU-B B05F650021), Thailand; Turkish Energy, Nuclear and Mineral Research Agency (TENMAK), Turkey; National Academy of Sciences of Ukraine, Ukraine; Science and Technology Facilities Council

(STFC), United Kingdom; National Science Foundation of the United States of America (NSF) and United States Department of Energy, Office of Nuclear Physics (DOE NP), United States of America. In addition, individual groups or members have received support from: Czech Science Foundation (grant no. 23-07499S), Czech Republic; European Research Council (grant no. 950692), European Union; ICSC – Centro Nazionale di Ricerca in High Performance Computing, Big Data and Quantum Computing, European Union – NextGenerationEU; Academy of Finland (Center of Excellence in Quark Matter) (grant nos. 346327, 346328), Finland.

Data Availability Statement This manuscript has associated data in a data repository. [Authors' comment: Manuscript has associated data in the HEPData repository at https://www.hepdata.net/record/ins2789570.]

Code Availability Statement This manuscript has no associated code/software. [Authors' comment: The code/software used for the analysis is publicly available on the github repository, at the links https://github.com/alisw/AliRoot and https://github.com/alisw/AliPhysics/.]

Funded by SCOAP[3].

References

1. J.C. Collins, D.E. Soper, G.F. Sterman, Factorization of hard processes in QCD. Adv. Ser. Direct. High Energy Phys. **5**, 1–91 (1989). https://doi.org/10.1142/9789814503266_0001. arXiv:hep-ph/0409313
2. M. Cacciari, M. Greco, P. Nason, The p_{T} spectrum in heavy flavor hadroproduction. JHEP **05**, 007 (1998). https://doi.org/10.1088/1126-6708/1998/05/007. arXiv:hep-ph/9803400
3. J. Altmann, A. Dubla, V. Greco, A. Rossi, P. Skands, Towards the understanding of heavy quarks hadronization: from leptonic to heavy-ion collisions. arXiv:2405.19137 [hep-ph]
4. G. Kramer, H. Spiesberger, Study of heavy meson production in p-Pb collisions at $\sqrt{s}$= 5.02 TeV in the general-mass variable-flavour-number scheme. Nucl. Phys. B **925**, 415–430 (2017). https://doi.org/10.1016/j.nuclphysb.2017.10.016. arXiv:1703.04754 [hep-ph]
5. I. Helenius, H. Paukkunen, Revisiting the D-meson hadroproduction in general-mass variable flavour number scheme. JHEP **05**, 196 (2018). https://doi.org/10.1007/JHEP05(2018)196. arXiv:1804.03557 [hep-ph]
6. M. Cacciari, S. Frixione, N. Houdeau, M.L. Mangano, P. Nason, G. Ridolfi, Theoretical predictions for charm and bottom production at the LHC. JHEP **10**, 137 (2012). https://doi.org/10.1007/JHEP10(2012)137. arXiv:1205.6344 [hep-ph]
7. M. Cacciari, M.L. Mangano, P. Nason, Gluon PDF constraints from the ratio of forward heavy-quark production at the LHC at $\sqrt{s}$ = 7 and 13 TeV. Eur. Phys. J. C **75**, 610 (2015). https://doi.org/10.1140/epjc/s10052-015-3814-x. arXiv:1507.06197 [hep-ph]
8. **ALICE** Collaboration, S. Acharya et al., The ALICE experiment—a journey through QCD. arXiv:2211.04384 [nucl-ex]
9. C.M.S. Collaboration, A. Tumasyan et al., Measurement of prompt open-charm production cross sections in proton-proton collisions at $\sqrt{s}$ = 13 TeV. JHEP **11**, 225 (2021). https://doi.org/10.1007/JHEP11(2021)225. arXiv:2107.01476 [hep-ex]
10. **LHCb** Collaboration, R. Aaij et al., Measurements of prompt charm production cross-sections in pp collisions at $\sqrt{s}$ = 5 TeV. JHEP **06**, 147 (2017). https://doi.org/10.1007/JHEP06(2017)147. arXiv:1610.02230 [hep-ex]
11. **LHCb** Collaboration, R. Aaij et al., Measurements of prompt charm production cross-sections in pp collisions at $\sqrt{s}$ = 13 TeV. JHEP **03**, 159 (2016). https://doi.org/10.1007/JHEP03(2016)159. arXiv:1510.01707 [hep-ex]. [Erratum: JHEP **09**, 013 (2016), Erratum: JHEP **05,** 074 (2017)]
12. S. Frixione, P. Nason, G. Ridolfi, A positive-weight next-to-leading-order Monte Carlo for heavy flavour hadroproduction. JHEP **09**, 126 (2007). https://doi.org/10.1088/1126-6708/2007/09/126. arXiv:0707.3088 [hep-ph]
13. T. Sjostrand, S. Mrenna, P.Z. Skands, PYTHIA 6.4 physics and manual. JHEP **05**, 026 (2006). https://doi.org/10.1088/1126-6708/2006/05/026. arXiv:hep-ph/0603175
14. **ALICE** Collaboration, S. Acharya et al., First measurement of Λ_{c}^{+} production down to p_{T} = 0 in pp and p–Pb collisions at $\sqrt{s_{\mathrm{NN}}}$ = 5.02 TeV. Phys. Rev. C **107**, 064901 (2023). https://doi.org/10.1103/PhysRevC.107.064901. arXiv:2211.14032 [nucl-ex]
15. **ALICE** Collaboration, S. Acharya et al., Measurement of beauty and charm production in pp collisions at $\sqrt{s}$ = 5.02 TeV via non-prompt and prompt D mesons. JHEP **05**, 220 (2021). https://doi.org/10.1007/JHEP05(2021)220. arXiv:2102.13601 [nucl-ex]
16. **ALICE** Collaboration, S. Acharya et al., Measurement of D-meson production at mid-rapidity in pp collisions at $\sqrt{s}$ = 7 TeV. Eur. Phys. J. C **77**, 550 (2017). https://doi.org/10.1140/epjc/s10052-017-5090-4. arXiv:1702.00766 [hep-ex]
17. **LHCb** Collaboration, R. Aaij et al., Observation of strangeness enhancement with charmed mesons in high-multiplicity pPb collisions at $\sqrt{s_{\mathrm{NN}}}$ = 8.16 TeV. arXiv:2311.08490 [hep-ex]
18. **ALICE** Collaboration, S. Acharya et al., Charm production and fragmentation fractions at midrapidity in pp collisions at $\sqrt{s}$ = 13 TeV. JHEP **12**, 086 (2023). https://doi.org/10.1007/JHEP12(2023)086. arXiv:2308.04877 [hep-ex]
19. **ALICE** Collaboration, J. Adam et al., D-meson production in p–Pb collisions at $\sqrt{s_{\mathrm{NN}}}$ = 5.02 TeV and in pp collisions at $\sqrt{s}$ = 7 TeV. Phys. Rev. C **94**, 054908 (2016). https://doi.org/10.1103/PhysRevC.94.054908. arXiv:1605.07569 [nucl-ex]
20. T. Sjöstrand, S. Ask, J.R. Christiansen, R. Corke, N. Desai, P. Ilten, S. Mrenna, S. Prestel, C.O. Rasmussen, P.Z. Skands, An introduction to PYTHIA 8.2. Comput. Phys. Commun. **191**, 159–177 (2015). https://doi.org/10.1016/j.cpc.2015.01.024. arXiv:1410.3012 [hep-ph]
21. P. Skands, S. Carrazza, J. Rojo, Tuning PYTHIA 8.1: the Monash 2013 Tune. Eur. Phys. J. C **74**, 3024 (2014). https://doi.org/10.1140/epjc/s10052-014-3024-y. arXiv:1404.5630 [hep-ph]
22. **ALICE** Collaboration, S. Acharya et al., Λ_{c}^{+} production in pp collisions at $\sqrt{s}$ = 7 TeV and in p–Pb collisions at $\sqrt{s_{\mathrm{NN}}}$ = 5.02 TeV. JHEP **04**, 108 (2018). https://doi.org/10.1007/JHEP04(2018)108. arXiv:1712.09581 [nucl-ex]
23. **ALICE** Collaboration, S. Acharya et al., Λ_{c}^{+} production in pp and in p–Pb collisions at $\sqrt{s_{\mathrm{NN}}}$ = 5.02 TeV. Phys. Rev. C **104**, 054905 (2021). https://doi.org/10.1103/PhysRevC.104.054905. arXiv:2011.06079 [nucl-ex]
24. **ALICE** Collaboration, S. Acharya et al., Λ_{c}^{+} production and baryon-to-meson ratios in pp and p–Pb collisions at $\sqrt{s_{\mathrm{NN}}}$ = 5.02 TeV at the LHC. Phys. Rev. Lett. **127**,

202301 (2021). https://doi.org/10.1103/PhysRevLett.127.202301. arXiv:2011.06078 [nucl-ex]
25. **CMS** Collaboration, A.M. Sirunyan et al., Production of Λ_c^+ baryons in proton-proton and lead-lead collisions at $\sqrt{s_{NN}} = 5.02$ TeV. Phys. Lett. B **803**, 135328 (2020). https://doi.org/10.1016/j.physletb.2020.135328. arXiv:1906.03322 [hep-ex]
26. **ALICE** Collaboration, S. Acharya et al., Measurement of the production cross section of prompt Ξ_c^0 baryons at midrapidity in pp collisions at $\sqrt{s} = 5.02$ TeV. JHEP **10**, 159 (2021). https://doi.org/10.1007/JHEP10(2021)159. arXiv:2105.05616 [nucl-ex]
27. **ALICE** Collaboration, S. Acharya et al., Measurement of the cross sections of Ξ_c^0 and Ξ_c^+ baryons and of the branching-fraction ratio $BR(\Xi_c^0 \rightarrow \Xi^- e^+ \nu_e)/BR(\Xi_c^0 \rightarrow \Xi^- \pi^+)$ in pp collisions at 13 TeV. Phys. Rev. Lett. **127**, 272001 (2021). https://doi.org/10.1103/PhysRevLett.127.272001. arXiv:2105.05187 [nucl-ex]
28. **ALICE** Collaboration, S. Acharya et al., Measurement of prompt D^0, Λ_c^+, and $\Sigma_c^{0,++}(2455)$ production in proton–proton collisions at $\sqrt{s} = 13$ TeV. Phys. Rev. Lett. **128**, 012001 (2022). https://doi.org/10.1103/PhysRevLett.128.012001. arXiv:2106.08278 [hep-ex]
29. **ALICE** Collaboration, S. Acharya et al., First measurement of Ω_c^0 production in pp collisions at $\sqrt{s} = 13$ TeV. Phys. Lett. B **846**, 137625 (2023). https://doi.org/10.1016/j.physletb.2022.137625. arXiv:2205.13993 [nucl-ex]
30. **LHCb** Collaboration, R. Aaij et al., Prompt Λ_c^+ production in pPb collisions at $\sqrt{s_{NN}} = 5.02$ TeV. JHEP **02**, 102 (2019). https://doi.org/10.1007/JHEP02(2019)102. arXiv:1809.01404 [hep-ex]
31. Y. Dai, S. Zhao, M. He, On the non-universality of heavy quark hadronization in elementary high-energy collisions. arXiv:2402.03692 [hep-ph]
32. J.R. Christiansen, P.Z. Skands, String formation beyond leading colour. JHEP **08**, 003 (2015). https://doi.org/10.1007/JHEP08(2015)003. arXiv:1505.01681 [hep-ph]
33. C. Bierlich, G. Gustafson, L. Lönnblad, H. Shah, The dynamic hadronization of charm quarks in heavy-ion collisions. Eur. Phys. J. C **84**, 231 (2024). https://doi.org/10.1140/epjc/s10052-024-12593-0. arXiv:2309.12452 [hep-ph]
34. V. Minissale, S. Plumari, V. Greco, Charm hadrons in pp collisions at LHC energy within a coalescence plus fragmentation approach. Phys. Lett. B **821**, 136622 (2021). https://doi.org/10.1016/j.physletb.2021.136622. arXiv:2012.12001 [hep-ph]
35. J. Song, H.-H. Li, F.-L. Shao, New feature of low p_T charm quark hadronization in pp collisions at $\sqrt{s} = 7$ TeV. Eur. Phys. J. C **78**, 344 (2018). https://doi.org/10.1140/epjc/s10052-018-5817-x. arXiv:1801.09402 [hep-ph]
36. A. Beraudo, A. De Pace, D. Pablos, F. Prino, M. Monteno, M. Nardi, Heavy-flavor transport and hadronization in pp collisions. arXiv:2306.02152 [hep-ph]
37. M. He, R. Rapp, Charm-baryon production in proton-proton collisions. Phys. Lett. B **795**, 117–121 (2019). https://doi.org/10.1016/j.physletb.2019.06.004. arXiv:1902.08889 [nucl-th]
38. **CMS** Collaboration, S. Chatrchyan et al., Measurement of the Λ_b cross section and the $\bar{\Lambda}_b$ to Λ_b ratio with $J/\Psi\Lambda$ decays in pp collisions at $\sqrt{s} = 7$ TeV. Phys. Lett. B **714**, 136–157 (2012). https://doi.org/10.1016/j.physletb.2012.05.063. arXiv:1205.0594 [hep-ex]
39. **LHCb** Collaboration, R. Aaij et al., Measurement of b hadron fractions in 13 TeV pp collisions. Phys. Rev. D **100**, 031102 (2019). https://doi.org/10.1103/PhysRevD.100.031102. arXiv:1902.06794 [hep-ex]
40. **LHCb** Collaboration, R. Aaij et al., Study of the production of Λ_b^0 and $\overline{B}^0$ hadrons in pp collisions and first measurement of the $\Lambda_b^0 \rightarrow J/\psi p K^-$ branching fraction. Chin. Phys. C **40**, 011001 (2016). https://doi.org/10.1088/1674-1137/40/1/011001. arXiv:1509.00292 [hep-ex]
41. **LHCb** Collaboration, R. Aaij et al., Measurement of B^+, B^0 and Λ_b^0 production in pPb collisions at $\sqrt{s_{NN}} = 8.16$ TeV. Phys. Rev. D **99** 052011 (2019). https://doi.org/10.1103/PhysRevD.99.052011. arXiv:1902.05599 [hep-ex]
42. **LHCb** Collaboration, R. Aaij et al., Enhanced Production of Λb0 Baryons in High-Multiplicity pp Collisions at s=13 TeV. Phys. Rev. Lett. **132**, 081901 (2024). https://doi.org/10.1103/PhysRevLett.132.081901. arXiv:2310.12278 [hep-ex]
43. **ALICE** Collaboration, S. Acharya et al., Study of flavor dependence of the baryon-to-meson ratio in proton-proton collisions at s=13 TeV. Phys. Rev. D **108**, 112003 (2023). https://doi.org/10.1103/PhysRevD.108.112003. arXiv:2308.04873 [hep-ex]
44. **ALICE** Collaboration, S. Acharya et al., Charm-quark fragmentation fractions and production cross section at midrapidity in pp collisions at the LHC. Phys. Rev. D **105**, L011103 (2022). https://doi.org/10.1103/PhysRevD.105.L011103. arXiv:2105.06335 [nucl-ex]
45. M. Arneodo, Nuclear effects in structure functions. Phys. Rep. **240**, 301–393 (1994). https://doi.org/10.1016/0370-1573(94)90048-5
46. S. Malace, D. Gaskell, D.W. Higinbotham, I. Cloet, The challenge of the EMC effect: existing data and future directions. Int. J. Mod. Phys. E **23**, 1430013 (2014). https://doi.org/10.1142/S0218301314300136. arXiv:1405.1270 [nucl-ex]
47. K.J. Eskola, H. Paukkunen, C.A. Salgado, EPS09: a new generation of NLO and LO nuclear parton distribution functions. JHEP **04**, 065 (2009). https://doi.org/10.1088/1126-6708/2009/04/065. arXiv:0902.4154 [hep-ph]
48. M. Hirai, S. Kumano, T.H. Nagai, Determination of nuclear parton distribution functions and their uncertainties in next-to-leading order. Phys. Rev. C **76**, 065207 (2007). https://doi.org/10.1103/PhysRevC.76.065207. arXiv:0709.3038 [hep-ph]
49. D. de Florian, R. Sassot, Nuclear parton distributions at next-to-leading order. Phys. Rev. D **69**, 074028 (2004). https://doi.org/10.1103/PhysRevD.69.074028. arXiv:hep-ph/0311227
50. F. Gelis, E. Iancu, J. Jalilian-Marian, R. Venugopalan, The color glass condensate. Annu. Rev. Nucl. Part. Sci. **60**, 463–489 (2010). https://doi.org/10.1146/annurev.nucl.010909.083629. arXiv:1002.0333 [hep-ph]
51. I. Vitev, Non-Abelian energy loss in cold nuclear matter. Phys. Rev. C **75**, 064906 (2007). https://doi.org/10.1103/PhysRevC.75.064906. arXiv:hep-ph/0703002
52. X.-N. Wang, Systematic study of high p_T hadron spectra in pp, p A and A A collisions from SPS to RHIC energies. Phys. Rev. C **61**, 064910 (2000). https://doi.org/10.1103/PhysRevC.61.064910. arXiv:nucl-th/9812021
53. B.Z. Kopeliovich, J. Nemchik, A. Schafer, A.V. Tarasov, Cronin effect in hadron production off nuclei. Phys. Rev. Lett. **88**, 232303 (2002). https://doi.org/10.1103/PhysRevLett.88.232303. arXiv:hep-ph/0201010
54. **ALICE** Collaboration, S. Acharya et al., Measurement of prompt D^0, D^+, D^{*+}, and D_s^+ production in p–Pb collisions at $\sqrt{s_{NN}}$ = 5.02 TeV. JHEP **12**, 092 (2019). https://doi.org/10.1007/JHEP12(2019)092. arXiv:1906.03425 [nucl-ex]
55. K.J. Eskola, P. Paakkinen, H. Paukkunen, C.A. Salgado, EPPS16: nuclear parton distributions with LHC data. Eur. Phys. J. C **77**, 163 (2017). https://doi.org/10.1140/epjc/s10052-017-4725-9. arXiv:1612.05741 [hep-ph]
56. **ALICE** Collaboration, B.B. Abelev et al., Multiplicity dependence of pion, kaon, proton and lambda production in p–Pb collisions at $\sqrt{s_{NN}}$ = 5.02 TeV. Phys. Lett. B **728**, 25–38 (2014). https://doi.org/10.1016/j.physletb.2013.11.020. arXiv:1307.6796 [nucl-ex]
57. **CMS** Collaboration, A.M. Sirunyan et al., Strange hadron production in pp and pPb collisions at $\sqrt{s_{NN}} = 5.02$ TeV. Phys. Rev. C **101**, 064906 (2020). https://doi.org/10.1103/PhysRevC.101.064906 . arXiv:1910.04812 [hep-ex]

58. T. Pierog, I. Karpenko, J.M. Katzy, E. Yatsenko, K. Werner, EPOS LHC: test of collective hadronization with data measured at the CERN Large Hadron Collider. Phys. Rev. C **92**, 034906 (2015). https://doi.org/10.1103/PhysRevC.92.034906. arXiv:1306.0121 [hep-ph]
59. E. Schnedermann, J. Sollfrank, U. Heinz, Thermal phenomenology of hadrons from 200-AGeV S+S collisions. Phys. Rev. C **48**, 2462–2475 (1993). https://doi.org/10.1103/PhysRevC.48.2462. arXiv:nucl-th/9307020
60. **ALICE** Collaboration, S. Acharya et al., Observation of a multiplicity dependence in the p_{T}-differential charm baryon-to-meson ratios in proton–proton collisions at $\sqrt{s_{\mathrm{NN}}} = 5.02$ TeV. Phys. Lett. B **829**, 137065 (2022). https://doi.org/10.1016/j.physletb.2022.137065. arXiv:2111.11948 [nucl-ex]
61. R.J. Fries et al., Hadronization in heavy ion collisions: recombination and fragmentation of partons. Phys. Rev. Lett. **90**, 202303 (2003). https://doi.org/10.1103/PhysRevLett.90.202303. arXiv:nucl-th/0301087
62. **ALICE** Collaboration, S. Acharya et al., Charm fragmentation fractions and $\mathrm{c\bar{c}}$ cross section in p–Pb collisions at $\sqrt{s_{\mathrm{NN}}} = 5.02$ TeV. arXiv:2405.14571 [nucl-ex]
63. **ALICE** Collaboration, K. Aamodt et al., The ALICE experiment at the CERN LHC. JINST **3**, S08002 (2008). https://doi.org/10.1088/1748-0221/3/08/S08002
64. **ALICE** Collaboration, B.B. Abelev et al., Performance of the ALICE Experiment at the CERN LHC. Int. J. Mod. Phys. A **29**, 1430044 (2014). https://doi.org/10.1142/S0217751X14300440. arXiv:1402.4476 [nucl-ex]
65. **ALICE** Collaboration, K. Aamodt et al., Alignment of the ALICE Inner Tracking System with cosmic-ray tracks. JINST **5**, P03003 (2010). https://doi.org/10.1088/1748-0221/5/03/P03003. arXiv:1001.0502 [physics.ins-det]
66. J. Alme et al., The ALICE TPC, a large 3-dimensional tracking device with fast readout for ultra-high multiplicity events. Nucl. Instr. Methods A **622**, 316–367 (2010). https://doi.org/10.1016/j.nima.2010.04.042. arXiv:1001.1950
67. A. Akindinov et al., Performance of the ALICE time-of-flight detector at the LHC. Eur. Phys. J. Plus **128**, 44 (2013). https://doi.org/10.1140/epjp/i2013-13044-x
68. **ALICE** Collaboration, E. Abbas et al., Performance of the ALICE VZERO system. JINST **8**, P10016 (2013). https://doi.org/10.1088/1748-0221/8/10/P10016. arXiv:1306.3130 [nucl-ex]
69. **ALICE** Collaboration, J. Adam et al., Determination of the event collision time with the ALICE detector at the LHC. Eur. Phys. J. Plus **132**, 99 (2017). https://doi.org/10.1140/epjp/i2017-11279-1. arXiv:1610.03055 [physics.ins-det]
70. **ALICE** Collaboration, S. Acharya et al., Pseudorapidity distributions of charged particles as a function of mid- and forward rapidity multiplicities in pp collisions at $\sqrt{s}$=5.02, 7 and 13 TeV. Eur. Phys. J. C **81**, 630 (2021). https://doi.org/10.1140/epjc/s10052-021-09349-5. arXiv:2009.09434 [nucl-ex]
71. **Particle Data Group** Collaboration, R.L. Workman et al., Review of particle physics. PTEP **2022**, 083C01 (2022). https://doi.org/10.1093/ptep/ptac097
72. **ALICE** Collaboration, S. Acharya et al., Multiplicity dependence of (multi-)strange hadron production in proton-proton collisions at $\sqrt{s}$ = 13 TeV. Eur. Phys. J. C **80**, 167 (2020). https://doi.org/10.1140/epjc/s10052-020-7673-8. arXiv:1908.01861 [nucl-ex]
73. **ALICE** Collaboration, S. Acharya et al., First measurement of Ξ_{c}^{0} production in pp collisions at $\sqrt{s}$ = 7 TeV. Phys. Lett. B **781**, 8–19 (2018). https://doi.org/10.1016/j.physletb.2018.03.061. arXiv:1712.04242 [hep-ex]
74. I. Kisel, I. Kulakov, M. Zyzak, Standalone first level event selection package for the CBM Experiment. IEEE Trans. Nucl. Sci. **60**, 3703–3708 (2013). https://doi.org/10.1109/TNS.2013.2265276
75. T. Chen, C. Guestrin, XGBoost: a scalable tree boosting system, in *Proceedings of the 22nd ACM SIGKDD International Conference on Knowledge Discovery and Data Mining*, pp. 785–794 (2016). https://doi.org/10.1145/2939672.2939785. arXiv:1603.02754 [cs.LG]
76. L. Barioglio, F. Catalano, M. Concas, P. Fecchio, F. Grosa, F. Mazzaschi, M. Puccio, hipe4ml/hipe4ml (2021). https://doi.org/10.5281/zenodo.5734093
77. X.-N. Wang, M. Gyulassy, HIJING: a Monte Carlo model for multiple jet production in pp, pA, and AA collisions. Phys. Rev. D **44**, 3501 (1991). https://doi.org/10.1103/PhysRevD.44.3501
78. R. Brun et al., GEANT: Detector Description and Simulation Tool; Oct 1994. CERN Program Library (CERN, Geneva, 1993). https://doi.org/10.17181/CERN.MUHF.DMJ1. http://cds.cern.ch/record/1082634. Long Writeup W5013
79. H. Li, F. Shao, J. Song, R. Wang, Production of single-charm hadrons by quark combination mechanism in p-Pb collisions at $\sqrt{s_{\mathrm{NN}}} = 5.02$ TeV. Rev. C **97**, 064915 (2018). https://doi.org/10.1103/PhysRevC.97.064915Phys. arXiv:1712.08921 [hep-ph]
80. M. Cacciari, P. Nason, R. Vogt, QCD predictions for charm and bottom production at RHIC. Phys. Rev. Lett. **95**, 122001 (2005). https://doi.org/10.1103/PhysRevLett.95.122001. arXiv:hep-ph/0502203
81. L. Gladilin, Fragmentation fractions of c and b quarks into charmed hadrons at LEP. Eur. Phys. J. C **75**, 19 (2015). https://doi.org/10.1140/epjc/s10052-014-3250-3. arXiv:1404.3888 [hep-ex]
82. **ALICE** Collaboration, B. Abelev et al., Measurement of visible cross sections in proton–lead collisions at $\sqrt{s_{\mathrm{NN}}}$ = 5.02 TeV in van der Meer scans with the ALICE detector. JINST **9**, P11003 (2014). https://doi.org/10.1088/1748-0221/9/11/P11003. arXiv:1405.1849 [nucl-ex]
83. S. Dulat et al., New parton distribution functions from a global analysis of quantum chromodynamics. Phys. Rev. D **93**, 033006 (2016). https://doi.org/10.1103/PhysRevD.93.033006. arXiv:1506.07443 [hep-ph]
84. A. Andronic, F. Beutler, P. Braun-Munzinger, K. Redlich, J. Stachel, Statistical hadronization of heavy flavor quarks in elementary collisions: successes and failures. Phys. Lett. B **678**, 350–354 (2009). https://doi.org/10.1016/j.physletb.2009.06.051. arXiv:0904.1368 [hep-ph]
85. R. Averbeck, N. Bastid, Z. C. del Valle, P. Crochet, A. Dainese, X. Zhang, Reference Heavy Flavour Cross Sections in pp Collisions at $\sqrt{s}$ = 2.76 TeV, using a pQCD-Driven $\sqrt{s}$-Scaling of ALICE Measurements at $\sqrt{s}$ = 7 TeV. arXiv:1107.3243 [hep-ph]
86. **LHCb** Collaboration, R. Aaij et al., Measurement of Ξ_c^+ production in pPb collisions at $\sqrt{s_{NN}} = 8.16$ TeV at LHCb. arXiv:2305.06711 [hep-ex]

ALICE Collaboration

S. Acharya[127], D. Adamová[86], A. Agarwal[135], G. Aglieri Rinella[32], L. Aglietta[24], M. Agnello[29], N. Agrawal[25], Z. Ahammed[135], S. Ahmad[15], S. U. Ahn[71], I. Ahuja[37], A. Akindinov[141], V. Akishina[38], M. Al-Turany[97], D. Aleksandrov[141], B. Alessandro[56], H. M. Alfanda[6], R. Alfaro Molina[67], B. Ali[15], A. Alici[25], N. Alizadehvandchali[116], A. Alkin[104], J. Alme[20], G. Alocco[52], T. Alt[64], A. R. Altamura[50], I. Altsybeev[95], J. R. Alvarado[44], C. O. R. Alvarez[44], M. N. Anaam[6], C. Andrei[45], N. Andreou[115], A. Andronic[126], E. Andronov[141], V. Anguelov[94], F. Antinori[54], P. Antonioli[51], N. Apadula[74], L. Aphecetche[103], H. Appelshäuser[64], C. Arata[73], S. Arcelli[25], M. Aresti[22], R. Arnaldi[56], J. G. M. C. A. Arneiro[110], I. C. Arsene[19], M. Arslandok[138], A. Augustinus[32], R. Averbeck[97], D. Averyanov[141], M. D. Azmi[15], H. Baba[124], A. Badalà[53], J. Bae[104], Y. W. Baek[40], X. Bai[120], R. Bailhache[64], Y. Bailung[48], R. Bala[91], A. Balbino[29], A. Baldisseri[130], B. Balis[2], D. Banerjee[4], Z. Banoo[91], V. Barbasova[37], F. Barile[31], L. Barioglio[56], M. Barlou[78], B. Barman[41], G. G. Barnaföldi[46], L. S. Barnby[115], E. Barreau[103], V. Barret[127], L. Barreto[110], C. Bartels[119], K. Barth[32], E. Bartsch[64], N. Bastid[127], S. Basu[75], G. Batigne[103], D. Battistini[95], B. Batyunya[142], D. Bauri[47], J. L. Bazo Alba[101], I. G. Bearden[83], C. Beattie[138], P. Becht[97], D. Behera[48], I. Belikov[129], A. D. C. Bell Hechavarria[126], F. Bellini[25], R. Bellwied[116], S. Belokurova[141], L. G. E. Beltran[109], Y. A. V. Beltran[44], G. Bencedi[46], A. Bensaoula[116], S. Beole[24], Y. Berdnikov[141], A. Berdnikova[94], L. Bergmann[94], M. G. Besoiu[63], L. Betev[32], P. P. Bhaduri[135], A. Bhasin[91], B. Bhattacharjee[41], L. Bianchi[24], N. Bianchi[49], J. Bielčík[35], J. Bielčíková[86], A. P. Bigot[129], A. Bilandzic[95], G. Biro[46], S. Biswas[4], N. Bize[103], J. T. Blair[108], D. Blau[141], M. B. Blidaru[97], N. Bluhme[38], C. Blume[64], G. Boca[21,55], F. Bock[87], T. Bodova[20], J. Bok[16], L. Boldizsár[46], M. Bombara[37], P. M. Bond[32], G. Bonomi[55,134], H. Borel[130], A. Borissov[141], A. G. Borquez Carcamo[94], H. Bossi[138], E. Botta[24], Y. E. M. Bouziani[64], L. Bratrud[64], P. Braun-Munzinger[97], M. Bregant[110], M. Broz[35], G. E. Bruno[31,96], V. D. Buchakchiev[36], M. D. Buckland[23], D. Budnikov[141], H. Buesching[64], S. Bufalino[29], P. Buhler[102], N. Burmasov[141], Z. Buthelezi[68,123], A. Bylinkin[20], S. A. Bysiak[107], J. C. Cabanillas Noris[109], M. F. T. Cabrera[116], M. Cai[6], H. Caines[138], A. Caliva[28], E. Calvo Villar[101], J. M. M. Camacho[109], P. Camerini[23], F. D. M. Canedo[110], S. L. Cantway[138], M. Carabas[113], A. A. Carballo[32], F. Carnesecchi[32], R. Caron[128], L. A. D. Carvalho[110], J. Castillo Castellanos[130], M. Castoldi[32], F. Catalano[32], S. Cattaruzzi[23], C. Ceballos Sanchez[142], R. Cerri[24], I. Chakaberia[74], P. Chakraborty[47,136], S. Chandra[135], S. Chapeland[32], M. Chartier[119], S. Chattopadhay[135], S. Chattopadhyay[135], S. Chattopadhyay[99], M. Chen[39], T. Cheng[6,97], C. Cheshkov[128], V. Chibante Barroso[32], D. D. Chinellato[111], F. Chinu[24], E. S. Chizzali[95,a], J. Cho[58], S. Cho[58], P. Chochula[32], Z. A. Chochulska[136], D. Choudhury[41], P. Christakoglou[84], C. H. Christensen[83], P. Christiansen[75], T. Chujo[125], M. Ciacco[29], C. Cicalo[52], M. R. Ciupek[97], G. Clai[51,b], F. Colamaria[50], J. S. Colburn[100], D. Colella[31], M. Colocci[25], M. Concas[32], G. Conesa Balbastre[73], Z. Conesa del Valle[131], G. Contin[23], J. G. Contreras[35], M. L. Coquet[103,130], P. Cortese[56,133], M. R. Cosentino[112], F. Costa[32], S. Costanza[21,55], C. Cot[131], J. Crkovská[94], P. Crochet[127], R. Cruz-Torres[74], P. Cui[6], M. M. Czarnynoga[136], A. Dainese[54], G. Dange[38], M. C. Danisch[94], A. Danu[63], P. Das[80], P. Das[4], S. Das[4], A. R. Dash[126], S. Dash[47], A. De Caro[28], G. de Cataldo[50], J. de Cuveland[38], A. De Falco[22], D. De Gruttola[28], N. De Marco[56], C. De Martin[23], S. De Pasquale[28], R. Deb[134], R. Del Grande[95], L. Dello Stritto[32], W. Deng[6], K. C. Devereaux[18], P. Dhankher[18], D. Di Bari[31], A. Di Mauro[32], B. Diab[130], R. A. Diaz[7,142], T. Dietel[114], Y. Ding[6], J. Ditzel[64], R. Divià[32], Ø. Djuvsland[20], U. Dmitrieva[141], A. Dobrin[63], B. Dönigus[64], J. M. Dubinski[136], A. Dubla[97], P. Dupieux[127], N. Dzalaiova[13], T. M. Eder[126], R. J. Ehlers[74], F. Eisenhut[64], R. Ejima[92], D. Elia[50], B. Erazmus[103], F. Ercolessi[25], B. Espagnon[131], G. Eulisse[32], D. Evans[100], S. Evdokimov[141], L. Fabbietti[95], M. Faggin[23], J. Faivre[73], F. Fan[6], W. Fan[74], A. Fantoni[49], M. Fasel[87], A. Feliciello[56], G. Feofilov[141], A. Fernández Téllez[44], L. Ferrandi[110], M. B. Ferrer[32], A. Ferrero[130], C. Ferrero[56,c], A. Ferretti[24], V. J. G. Feuillard[94], V. Filova[35], D. Finogeev[141], F. M. Fionda[52], E. Flatland[32], F. Flor[116,138], A. N. Flores[108], S. Foertsch[68], I. Fokin[94], S. Fokin[141], U. Follo[56,c], E. Fragiacomo[57], E. Frajna[46], U. Fuchs[32], N. Funicello[28], C. Furget[73], A. Furs[141], T. Fusayasu[98], J. J. Gaardhøje[83], M. Gagliardi[24], A. M. Gago[101], T. Gahlaut[47], C. D. Galvan[109], D. R. Gangadharan[116], P. Ganoti[78], C. Garabatos[97], J. M. Garcia[44], T. García Chávez[44], E. Garcia-Solis[9], C. Gargiulo[32], P. Gasik[97], H. M. Gaur[38], A. Gautam[118], M. B. Gay Ducati[66], M. Germain[103], C. Ghosh[135], M. Giacalone[51], G. Gioachin[29], P. Giubellino[56,97], P. Giubilato[27], A. M. C. Glaenzer[130], P. Glässel[94], E. Glimos[122], D. J. Q. Goh[76], V. Gonzalez[137], P. Gordeev[141], M. Gorgon[2], K. Goswami[48], S. Gotovac[33], V. Grabski[67],

L. K. Graczykowski[136], E. Grecka[86], A. Grelli[59], C. Grigoras[32], V. Grigoriev[141], S. Grigoryan[1,142], F. Grosa[32], J. F. Grosse-Oetringhaus[32], R. Grosso[97], D. Grund[35], N. A. Grunwald[94], G. G. Guardiano[111], R. Guernane[73], M. Guilbaud[103], K. Gulbrandsen[83], J. J. W. K. Gumprecht[102], T. Gündem[64], T. Gunji[124], W. Guo[6], A. Gupta[91], R. Gupta[91], R. Gupta[48], K. Gwizdziel[136], L. Gyulai[46], C. Hadjidakis[131], F. U. Haider[91], S. Haidlova[35], M. Haldar[4], H. Hamagaki[76], A. Hamdi[74], Y. Han[139], B. G. Hanley[137], R. Hannigan[108], J. Hansen[75], M. R. Haque[97], J. W. Harris[138], A. Harton[9], M. V. Hartung[64], H. Hassan[117], D. Hatzifotiadou[51], P. Hauer[42], L. B. Havener[138], E. Hellbär[97], H. Helstrup[34], M. Hemmer[64], T. Herman[35], S. G. Hernandez[116], G. Herrera Corral[8], S. Herrmann[128], K. F. Hetland[34], B. Heybeck[64], H. Hillemanns[32], B. Hippolyte[129], F. W. Hoffmann[70], B. Hofman[59], G. H. Hong[139], M. Horst[95], A. Horzyk[2], Y. Hou[6], P. Hristov[32], P. Huhn[64], L. M. Huhta[117], T. J. Humanic[88], A. Hutson[116], D. Hutter[38], M. C. Hwang[18], R. Ilkaev[141], M. Inaba[125], G. M. Innocenti[32], M. Ippolitov[141], A. Isakov[84], T. Isidori[118], M. S. Islam[99], S. Iurchenko[141], M. Ivanov[13], M. Ivanov[97], V. Ivanov[141], K. E. Iversen[75], M. Jablonski[2], B. Jacak[18,74], N. Jacazio[25], P. M. Jacobs[74], S. Jadlovska[106], J. Jadlovsky[106], S. Jaelani[82], C. Jahnke[110], M. J. Jakubowska[136], M. A. Janik[136], T. Janson[70], S. Ji[16], S. Jia[10], A. A. P. Jimenez[65], F. Jonas[74], D. M. Jones[119], J. M. Jowett[32,97], J. Jung[64], M. Jung[64], A. Junique[32], A. Jusko[100], J. Kaewjai[105], P. Kalinak[60], A. Kalweit[32], A. Karasu Uysal[72,d], D. Karatovic[89], N. Karatzenis[100], O. Karavichev[141], T. Karavicheva[141], E. Karpechev[141], M. J. Karwowska[32,136], U. Kebschull[70], R. Keidel[140], M. Keil[32], B. Ketzer[42], S. S. Khade[48], A. M. Khan[120], S. Khan[15], A. Khanzadeev[141], Y. Kharlov[141], A. Khatun[118], A. Khuntia[35], Z. Khuranova[64], B. Kileng[34], B. Kim[104], C. Kim[16], D. J. Kim[117], E. J. Kim[69], J. Kim[139], J. Kim[58], J. Kim[32,69], M. Kim[18], S. Kim[17], T. Kim[139], K. Kimura[92], A. Kirkova[36], S. Kirsch[64], I. Kisel[38], S. Kiselev[141], A. Kisiel[136], J. P. Kitowski[2], J. L. Klay[5], J. Klein[32], S. Klein[74], C. Klein-Bösing[126], M. Kleiner[64], T. Klemenz[95], A. Kluge[32], C. Kobdaj[105], R. Kohara[124], T. Kollegger[97], A. Kondratyev[142], N. Kondratyeva[141], J. Konig[64], S. A. Konigstorfer[95], P. J. Konopka[32], G. Kornakov[136], M. Korwieser[95], S. D. Koryciak[2], C. Koster[84], A. Kotliarov[86], N. Kovacic[89], V. Kovalenko[141], M. Kowalski[107], V. Kozhuharov[36], I. Králik[60], A. Kravčáková[37], L. Krcal[32,38], M. Krivda[100,60], F. Krizek[86], K. Krizkova Gajdosova[32], C. Krug[66], M. Krüger[64], D. M. Krupova[35], E. Kryshen[141], V. Kučera[58], C. Kuhn[129], P. G. Kuijer[84], T. Kumaoka[125], D. Kumar[135], L. Kumar[90], N. Kumar[90], S. Kumar[31], S. Kundu[32], P. Kurashvili[79], A. Kurepin[141], A. B. Kurepin[141], A. Kuryakin[141], S. Kushpil[86], V. Kuskov[141], M. Kutyla[136], A. Kuznetsov[142], M. J. Kweon[58], Y. Kwon[139], S. L. La Pointe[38], P. La Rocca[26], A. Lakrathok[105], M. Lamanna[32], A. R. Landou[73], R. Langoy[121], P. Larionov[32], E. Laudi[32], L. Lautner[32,95], R. A. N. Laveaga[109], R. Lavicka[102], R. Lea[55,134], H. Lee[104], I. Legrand[45], G. Legras[126], J. Lehrbach[38], A. M. Lejeune[35], T. M. Lelek[2], R. C. Lemmon[85,*], I. León Monzón[109], M. M. Lesch[95], E. D. Lesser[18], P. Lévai[46], M. Li[6], X. Li[10], B. E. Liang-gilman[18], J. Lien[121], R. Lietava[100], I. Likmeta[116], B. Lim[24], S. H. Lim[16], V. Lindenstruth[38], A. Lindner[45], C. Lippmann[97], D. H. Liu[6], J. Liu[119], G. S. S. Liveraro[111], I. M. Lofnes[20], C. Loizides[87], S. Lokos[107], J. Lömker[59], X. Lopez[127], E. López Torres[7], C. Lotteau[128], P. Lu[97,120], F. V. Lugo[67], J. R. Luhder[126], M. Lunardon[27], G. Luparello[57], Y. G. Ma[39], M. Mager[32], A. Maire[129], E. M. Majerz[2], M. V. Makariev[36], M. Malaev[141], G. Malfattore[25], N. M. Malik[91], Q. W. Malik[19], S. K. Malik[91], L. Malinina[142,g,*], D. Mallick[131], N. Mallick[48], G. Mandaglio[30,53], S. K. Mandal[79], A. Manea[63], V. Manko[141], F. Manso[127], V. Manzari[50], Y. Mao[6], R. W. Marcjan[2], G. V. Margagliotti[23], A. Margotti[51], A. Marín[97], C. Markert[108], P. Martinengo[32], M. I. Martínez[44], G. Martínez García[103], M. P. P. Martins[110], S. Masciocchi[97], M. Masera[24], A. Masoni[52], L. Massacrier[131], O. Massen[59], A. Mastroserio[50,132], O. Matonoha[75], S. Mattiazzo[27], A. Matyja[107], A. L. Mazuecos[32], F. Mazzaschi[24,32], M. Mazzilli[116], J. E. Mdhluli[123], Y. Melikyan[43], M. Melo[110], A. Menchaca-Rocha[67], J. E. M. Mendez[65], E. Meninno[102], A. S. Menon[116], M. W. Menzel[32,94], M. Meres[13], Y. Miake[125], L. Micheletti[32], D. L. Mihaylov[95], K. Mikhaylov[141,142], N. Minafra[118], D. Miśkowiec[97], A. Modak[4,134], B. Mohanty[80], M. Mohisin Khan[15,e], M. A. Molander[43], S. Monira[136], C. Mordasini[117], D. A. Moreira De Godoy[126], I. Morozov[141], A. Morsch[32], T. Mrnjavac[32], V. Muccifora[49], S. Muhuri[135], J. D. Mulligan[74], A. Mulliri[22], M. G. Munhoz[110], R. H. Munzer[64], H. Murakami[124], S. Murray[114], L. Musa[32], J. Musinsky[60], J. W. Myrcha[136], B. Naik[123], A. I. Nambrath[18], B. K. Nandi[47], R. Nania[51], E. Nappi[50], A. F. Nassirpour[17], A. Nath[94], C. Nattrass[122], M. N. Naydenov[36], A. Neagu[19], A. Negru[113], E. Nekrasova[141], L. Nellen[65], R. Nepeivoda[75], S. Nese[19], G. Neskovic[38], N. Nicassio[50], B. S. Nielsen[83], E. G. Nielsen[83], S. Nikolaev[141], S. Nikulin[141], V. Nikulin[141], F. Noferini[51], S. Noh[12], P. Nomokonov[142], J. Norman[119], N. Novitzky[87], P. Nowakowski[136], A. Nyanin[141], J. Nystrand[20], S. Oh[17], A. Ohlson[75], V. A. Okorokov[141], J. Oleniacz[136], A. Onnerstad[117], C. Oppedisano[56], A. Ortiz Velasquez[65],

J. Otwinowski[107], M. Oya[92], K. Oyama[76], Y. Pachmayer[94], S. Padhan[47], D. Pagano[55,134], G. Paić[65], S. Paisano-Guzmán[44], A. Palasciano[50], S. Panebianco[130], C. Pantouvakis[27], H. Park[125], H. Park[104], J. Park[125], J. E. Parkkila[32], Y. Patley[47], B. Paul[22], H. Pei[6], T. Peitzmann[59], X. Peng[11], M. Pennisi[24], S. Perciballi[24], D. Peresunko[141], G. M. Perez[7], Y. Pestov[141], M. T. Petersen[83], V. Petrov[141], M. Petrovici[45], S. Piano[57], M. Pikna[13], P. Pillot[103], O. Pinazza[32,51], L. Pinsky[116], C. Pinto[95], S. Pisano[49], M. Płoskoń[74], M. Planinic[89], F. Pliquett[64], D. K. Plociennik[2], M. G. Poghosyan[87], B. Polichtchouk[141], S. Politano[29], N. Poljak[89], A. Pop[45], S. Porteboeuf-Houssais[127], V. Pozdniakov[142,*], I. Y. Pozos[44], K. K. Pradhan[48], S. K. Prasad[4], S. Prasad[48], R. Preghenella[51], F. Prino[56], C. A. Pruneau[137], I. Pshenichnov[141], M. Puccio[32], S. Pucillo[24], S. Qiu[84], L. Quaglia[24], S. Ragoni[14], A. Rai[138], A. Rakotozafindrabe[130], L. Ramello[56,133], F. Rami[129], M. Rasa[26], S. S. Räsänen[43], R. Rath[51], M. P. Rauch[20], I. Ravasenga[32], K. F. Read[87,122], C. Reckziegel[112], A. R. Redelbach[38], K. Redlich[79,f], C. A. Reetz[97], H. D. Regules-Medel[44], A. Rehman[20], F. Reidt[32], H. A. Reme-Ness[34], Z. Rescakova[37], K. Reygers[94], A. Riabov[141], V. Riabov[141], R. Ricci[28], M. Richter[20], A. A. Riedel[95], W. Riegler[32], A. G. Riffero[24], M. Rignanese[27], C. Ripoli[28], C. Ristea[63], M. V. Rodriguez[32], M. Rodríguez Cahuantzi[44], S. A. Rodríguez Ramírez[44], K. Røed[19], R. Rogalev[141], E. Rogochaya[142], T. S. Rogoschinski[64], D. Rohr[32], D. Röhrich[20], S. Rojas Torres[35], P. S. Rokita[136], G. Romanenko[25], F. Ronchetti[49], E. D. Rosas[65], K. Roslon[136], A. Rossi[54], A. Roy[48], S. Roy[47], N. Rubini[25], J. A. Rudolph[84], D. Ruggiano[136], R. Rui[23], P. G. Russek[2], R. Russo[84], A. Rustamov[81], E. Ryabinkin[141], Y. Ryabov[141], A. Rybicki[107], J. Ryu[16], W. Rzesa[136], S. Sadhu[31], S. Sadovsky[141], J. Saetre[20], K. Šafařík[35], S. K. Saha[4], S. Saha[80], B. Sahoo[48], R. Sahoo[48], S. Sahoo[61], D. Sahu[48], P. K. Sahu[61], J. Saini[135], K. Sajdakova[37], S. Sakai[125], M. P. Salvan[97], S. Sambyal[91], D. Samitz[102], I. Sanna[32,95], T. B. Saramela[110], D. Sarkar[83], P. Sarma[41], V. Sarritzu[22], V. M. Sarti[95], M. H. P. Sas[32], S. Sawan[80], E. Scapparone[51], J. Schambach[87], H. S. Scheid[64], C. Schiaua[45], R. Schicker[94], F. Schlepper[94], A. Schmah[97], C. Schmidt[97], H. R. Schmidt[93], M. O. Schmidt[32], M. Schmidt[93], N. V. Schmidt[87], A. R. Schmier[122], R. Schotter[129], A. Schröter[38], J. Schukraft[32], K. Schweda[97], G. Scioli[25], E. Scomparin[56], J. E. Seger[14], Y. Sekiguchi[124], D. Sekihata[124], M. Selina[84], I. Selyuzhenkov[97], S. Senyukov[129], J. J. Seo[94], D. Serebryakov[141], L. Serkin[65], L. Šerkšnytė[95], A. Sevcenco[63], T. J. Shaba[68], A. Shabetai[103], R. Shahoyan[32], A. Shangaraev[141], B. Sharma[91], D. Sharma[47], H. Sharma[54], M. Sharma[91], S. Sharma[76], S. Sharma[91], U. Sharma[91], A. Shatat[131], O. Sheibani[116], K. Shigaki[92], M. Shimomura[77], J. Shin[12], S. Shirinkin[141], Q. Shou[39], Y. Sibiriak[141], S. Siddhanta[52], T. Siemiarczuk[79], T. F. Silva[110], D. Silvermyr[75], T. Simantathammakul[105], R. Simeonov[36], B. Singh[91], B. Singh[95], K. Singh[48], R. Singh[80], R. Singh[91], R. Singh[97], S. Singh[15], V. K. Singh[135], V. Singhal[135], T. Sinha[99], B. Sitar[13], M. Sitta[133,56], T. B. Skaali[19], G. Skorodumovs[94], N. Smirnov[138], R. J. M. Snellings[59], E. H. Solheim[19], J. Song[16], C. Sonnabend[32,97], J. M. Sonneveld[84], F. Soramel[27], A. B. Soto-hernandez[88], R. Spijkers[84], I. Sputowska[107], J. Staa[75], J. Stachel[94], I. Stan[63], P. J. Steffanic[122], S. F. Stiefelmaier[94], D. Stocco[103], I. Storehaug[19], N. J. Strangmann[64], P. Stratmann[126], S. Strazzi[25], A. Sturniolo[30,53], C. P. Stylianidis[84], A. A. P. Suaide[110], C. Suire[131], M. Sukhanov[141], M. Suljic[32], R. Sultanov[141], V. Sumberia[91], S. Sumowidagdo[82], I. Szarka[13], M. Szymkowski[136], S. F. Taghavi[95], G. Taillepied[97], J. Takahashi[111], G. J. Tambave[80], S. Tang[6], Z. Tang[120], J. D. Tapia Takaki[118], N. Tapus[113], L. A. Tarasovicova[126], M. G. Tarzila[45], G. F. Tassielli[31], A. Tauro[32], A. Tavira García[131], G. Tejeda Muñoz[44], A. Telesca[32], L. Terlizzi[24], C. Terrevoli[50], S. Thakur[4], D. Thomas[108], A. Tikhonov[141], N. Tiltmann[32,126], A. R. Timmins[116], M. Tkacik[106], T. Tkacik[106], A. Toia[64], R. Tokumoto[92], S. Tomassini[25], K. Tomohiro[92], N. Topilskaya[141], M. Toppi[49], V. V. Torres[103], A. G. Torres Ramos[31], A. Trifiró[30,53], T. Triloki[96], A. S. Triolo[30,32,53], S. Tripathy[32], T. Tripathy[47], V. Trubnikov[3], W. H. Trzaska[117], T. P. Trzcinski[136], C. Tsolanta[19], R. Tu[39], A. Tumkin[141], R. Turrisi[54], T. S. Tveter[19], K. Ullaland[20], B. Ulukutlu[95], A. Uras[128], M. Urioni[134], G. L. Usai[22], M. Vala[37], N. Valle[55], L. V. R. van Doremalen[59], M. van Leeuwen[84], C. A. van Veen[94], R. J. G. van Weelden[84], P. Vande Vyvre[32], D. Varga[46], Z. Varga[46], P. Vargas Torres[65], M. Vasileiou[78], A. Vasiliev[141], O. Vázquez Doce[49], O. Vazquez Rueda[116], V. Vechernin[141], E. Vercellin[24], S. Vergara Limón[44], R. Verma[47], L. Vermunt[97], R. Vértesi[46], M. Verweij[59], L. Vickovic[33], Z. Vilakazi[123], O. Villalobos Baillie[100], A. Villani[23], A. Vinogradov[141], T. Virgili[28], M. M. O. Virta[117], A. Vodopyanov[142], B. Volkel[32], M. A. Völkl[94], S. A. Voloshin[137], G. Volpe[31], B. von Haller[32], I. Vorobyev[32], N. Vozniuk[141], J. Vrláková[37], J. Wan[39], C. Wang[39], D. Wang[39], Y. Wang[39], Y. Wang[6], A. Wegrzynek[32], F. T. Weiglhofer[38], S. C. Wenzel[32], J. P. Wessels[126], J. Wiechula[64], J. Wikne[19], G. Wilk[79], J. Wilkinson[97], G. A. Willems[126], B. Windelband[94], M. Winn[130], J. R. Wright[108], W. Wu[39], Y. Wu[120], Z. Xiong[120], R. Xu[6], A. Yadav[42], A. K. Yadav[135], Y. Yamaguchi[92], S. Yang[20], S. Yano[92], E. R. Yeats[18], Z. Yin[6], I.-K. Yoo[16], J. H. Yoon[58],

H. Yu[12], S. Yuan[20], A. Yuncu[94], V. Zaccolo[23], C. Zampolli[32], M. Zang[6], F. Zanone[94], N. Zardoshti[32], A. Zarochentsev[141], P. Závada[62], N. Zaviyalov[141], M. Zhalov[141], B. Zhang[6], C. Zhang[130], L. Zhang[39], M. Zhang[6,127], S. Zhang[39], X. Zhang[6], Y. Zhang[120], Z. Zhang[6], M. Zhao[10], V. Zherebchevskii[141], Y. Zhi[10], D. Zhou[6], Y. Zhou[83], J. Zhu[6,54], S. Zhu[120], Y. Zhu[6], S. C. Zugravel[56], N. Zurlo[55,134]

[1] A.I. Alikhanyan National Science Laboratory (Yerevan Physics Institute) Foundation, Yerevan, Armenia
[2] AGH University of Krakow, Cracow, Poland
[3] Bogolyubov Institute for Theoretical Physics, National Academy of Sciences of Ukraine, Kiev, Ukraine
[4] Bose Institute, Department of Physics and Centre for Astroparticle Physics and Space Science (CAPSS), Kolkata, India
[5] California Polytechnic State University, San Luis Obispo, CA, USA
[6] Central China Normal University, Wuhan, China
[7] Centro de Aplicaciones Tecnológicas y Desarrollo Nuclear (CEADEN), Havana, Cuba
[8] Centro de Investigación y de Estudios Avanzados (CINVESTAV), Mexico City and Mérida, Mexico
[9] Chicago State University, Chicago, Illinois, United States
[10] China Institute of Atomic Energy, Beijing, China
[11] China University of Geosciences, Wuhan, China
[12] Chungbuk National University, Cheongju, Republic of Korea
[13] Faculty of Mathematics, Physics and Informatics, Comenius University Bratislava, Bratislava, Slovak Republic
[14] Creighton University, Omaha, NE, USA
[15] Department of Physics, Aligarh Muslim University, Aligarh, India
[16] Department of Physics, Pusan National University, Pusan, Republic of Korea
[17] Department of Physics, Sejong University, Seoul, Republic of Korea
[18] Department of Physics, University of California, Berkeley, CA, USA
[19] Department of Physics, University of Oslo, Oslo, Norway
[20] Department of Physics and Technology, University of Bergen, Bergen, Norway
[21] Dipartimento di Fisica, Università di Pavia, Pavia, Italy
[22] Dipartimento di Fisica dell'Università and Sezione INFN, Cagliari, Italy
[23] Dipartimento di Fisica dell'Università and Sezione INFN, Trieste, Italy
[24] Dipartimento di Fisica dell'Università and Sezione INFN, Turin, Italy
[25] Dipartimento di Fisica e Astronomia dell'Università and Sezione INFN, Bologna, Italy
[26] Dipartimento di Fisica e Astronomia dell'Università and Sezione INFN, Catania, Italy
[27] Dipartimento di Fisica e Astronomia dell'Università and Sezione INFN, Padua, Italy
[28] Dipartimento di Fisica 'E.R. Caianiello' dell'Università and Gruppo Collegato INFN, Salerno, Italy
[29] Dipartimento DISAT del Politecnico and Sezione INFN, Turin, Italy
[30] Dipartimento di Scienze MIFT, Università di Messina, Messina, Italy
[31] Dipartimento Interateneo di Fisica 'M. Merlin' and Sezione INFN, Bari, Italy
[32] European Organization for Nuclear Research (CERN), Geneva, Switzerland
[33] Faculty of Electrical Engineering, Mechanical Engineering and Naval Architecture, University of Split, Split, Croatia
[34] Faculty of Engineering and Science, Western Norway University of Applied Sciences, Bergen, Norway
[35] Faculty of Nuclear Sciences and Physical Engineering, Czech Technical University in Prague, Prague, Czech Republic
[36] Faculty of Physics, Sofia University, Sofia, Bulgaria
[37] Faculty of Science, P.J. Šafárik University, Kosice, Slovak Republic
[38] Frankfurt Institute for Advanced Studies, Johann Wolfgang Goethe-Universität Frankfurt, Frankfurt, Germany
[39] Fudan University, Shanghai, China
[40] Gangneung-Wonju National University, Gangneung, Republic of Korea
[41] Department of Physics, Gauhati University, Guwahati, India
[42] Helmholtz-Institut für Strahlen- und Kernphysik, Rheinische Friedrich-Wilhelms-Universität Bonn, Bonn, Germany
[43] Helsinki Institute of Physics (HIP), Helsinki, Finland
[44] High Energy Physics Group, Universidad Autónoma de Puebla, Puebla, Mexico
[45] Horia Hulubei National Institute of Physics and Nuclear Engineering, Bucharest, Romania
[46] HUN-REN Wigner Research Centre for Physics, Budapest, Hungary
[47] Indian Institute of Technology Bombay (IIT), Mumbai, India
[48] Indian Institute of Technology Indore, Indore, India

[49] INFN, Laboratori Nazionali di Frascati, Frascati, Italy
[50] INFN, Sezione di Bari, Bari, Italy
[51] INFN, Sezione di Bologna, Bologna, Italy
[52] INFN, Sezione di Cagliari, Cagliari, Italy
[53] INFN, Sezione di Catania, Catania, Italy
[54] INFN, Sezione di Padova, Padua, Italy
[55] INFN, Sezione di Pavia, Pavia, Italy
[56] INFN, Sezione di Torino, Turin, Italy
[57] INFN, Sezione di Trieste, Trieste, Italy
[58] Inha University, Incheon, Republic of Korea
[59] Institute for Gravitational and Subatomic Physics (GRASP), Utrecht University/Nikhef, Utrecht, Netherlands
[60] Institute of Experimental Physics, Slovak Academy of Sciences, Kosice, Slovak Republic
[61] Institute of Physics, Homi Bhabha National Institute, Bhubaneswar, India
[62] Institute of Physics of the Czech Academy of Sciences, Prague, Czech Republic
[63] Institute of Space Science (ISS), Bucharest, Romania
[64] Institut für Kernphysik, Johann Wolfgang Goethe-Universität Frankfurt, Frankfurt, Germany
[65] Instituto de Ciencias Nucleares, Universidad Nacional Autónoma de México, Mexico City, Mexico
[66] Instituto de Física, Universidade Federal do Rio Grande do Sul (UFRGS), Porto Alegre, Brazil
[67] Instituto de Física, Universidad Nacional Autónoma de México, Mexico City, Mexico
[68] iThemba LABS, National Research Foundation, Somerset West, South Africa
[69] Jeonbuk National University, Jeonju, Republic of Korea
[70] Johann-Wolfgang-Goethe Universität Frankfurt Institut für Informatik, Fachbereich Informatik und Mathematik, Frankfurt, Germany
[71] Korea Institute of Science and Technology Information, Daejeon, Republic of Korea
[72] KTO Karatay University, Konya, Turkey
[73] Laboratoire de Physique Subatomique et de Cosmologie, CNRS-IN2P3, Université Grenoble-Alpes, Grenoble, France
[74] Lawrence Berkeley National Laboratory, Berkeley, CA, USA
[75] Division of Particle Physics, Department of Physics, Lund University, Lund, Sweden
[76] Nagasaki Institute of Applied Science, Nagasaki, Japan
[77] Nara Women's University (NWU), Nara, Japan
[78] Department of Physics, School of Science, National and Kapodistrian University of Athens, Athens, Greece
[79] National Centre for Nuclear Research, Warsaw, Poland
[80] National Institute of Science Education and Research, Homi Bhabha National Institute, Jatni, India
[81] National Nuclear Research Center, Baku, Azerbaijan
[82] National Research and Innovation Agency-BRIN, Jakarta, Indonesia
[83] Niels Bohr Institute, University of Copenhagen, Copenhagen, Denmark
[84] Nikhef, National Institute for Subatomic Physics, Amsterdam, Netherlands
[85] Nuclear Physics Group, STFC Daresbury Laboratory, Daresbury, UK
[86] Nuclear Physics Institute of the Czech Academy of Sciences, Husinec-Řež, Czech Republic
[87] Oak Ridge National Laboratory, Oak Ridge, TN, USA
[88] Ohio State University, Columbus, OH, USA
[89] Physics department, Faculty of science, University of Zagreb, Zagreb, Croatia
[90] Physics Department, Panjab University, Chandigarh, India
[91] Physics Department, University of Jammu, Jammu, India
[92] Physics Program and International Institute for Sustainability with Knotted Chiral Meta Matter (SKCM2), Hiroshima University, Hiroshima, Japan
[93] Physikalisches Institut, Eberhard-Karls-Universität Tübingen, Tübingen, Germany
[94] Physikalisches Institut, Ruprecht-Karls-Universität Heidelberg, Heidelberg, Germany
[95] Physik Department, Technische Universität München, Munich, Germany
[96] Politecnico di Bari and Sezione INFN, Bari, Italy
[97] Research Division and ExtreMe Matter Institute EMMI, GSI Helmholtzzentrum für Schwerionenforschung GmbH, Darmstadt, Germany
[98] Saga University, Saga, Japan

[99] Saha Institute of Nuclear Physics, Homi Bhabha National Institute, Kolkata, India
[100] School of Physics and Astronomy, University of Birmingham, Birmingham, UK
[101] Sección Física, Departamento de Ciencias, Pontificia Universidad Católica del Perú, Lima, Peru
[102] Stefan Meyer Institut für Subatomare Physik (SMI), Vienna, Austria
[103] SUBATECH, IMT Atlantique, CNRS-IN2P3, Nantes Université, Nantes, France
[104] Sungkyunkwan University, Suwon City, Republic of Korea
[105] Suranaree University of Technology, Nakhon Ratchasima, Thailand
[106] Technical University of Košice, Kosice, Slovak Republic
[107] The Henryk Niewodniczanski Institute of Nuclear Physics, Polish Academy of Sciences, Cracow, Poland
[108] The University of Texas at Austin, Austin, TX, USA
[109] Universidad Autónoma de Sinaloa, Culiacán, Mexico
[110] Universidade de São Paulo (USP), São Paulo, Brazil
[111] Universidade Estadual de Campinas (UNICAMP), Campinas, Brazil
[112] Universidade Federal do ABC, Santo Andre, Brazil
[113] Universitatea Nationala de Stiinta si Tehnologie Politehnica Bucuresti, Bucharest, Romania
[114] University of Cape Town, Cape Town, South Africa
[115] University of Derby, Derby, UK
[116] University of Houston, Houston, TX, USA
[117] University of Jyväskylä, Jyvaskyla, Finland
[118] University of Kansas, Lawrence, KS, USA
[119] University of Liverpool, Liverpool, UK
[120] University of Science and Technology of China, Hefei, China
[121] University of South-Eastern Norway, Kongsberg, Norway
[122] University of Tennessee, Knoxville, TN, USA
[123] University of the Witwatersrand, Johannesburg, South Africa
[124] University of Tokyo, Tokyo, Japan
[125] University of Tsukuba, Tsukuba, Japan
[126] Universität Münster, Institut für Kernphysik, Münster, Germany
[127] CNRS/IN2P3, LPC, Université Clermont Auvergne, Clermont-Ferrand, France
[128] CNRS/IN2P3, Institut de Physique des 2 Infinis de Lyon, Université de Lyon, Lyon, France
[129] CNRS, IPHC UMR 7178, Université de Strasbourg, 67000 Strasbourg, France
[130] Départment de Physique Nucléaire (DPhN), Centre d'Etudes de Saclay (CEA), IRFU, Université Paris-Saclay, Saclay, France
[131] CNRS/IN2P3, IJCLab, Université Paris-Saclay, Orsay, France
[132] Università degli Studi di Foggia, Foggia, Italy
[133] Università del Piemonte Orientale, Vercelli, Italy
[134] Università di Brescia, Brescia, Italy
[135] Variable Energy Cyclotron Centre, Homi Bhabha National Institute, Kolkata, India
[136] Warsaw University of Technology, Warsaw, Poland
[137] Wayne State University, Detroit, MI, USA
[138] Yale University, New Haven, CT, USA
[139] Yonsei University, Seoul, Republic of Korea
[140] Zentrum für Technologie und Transfer (ZTT), Worms, Germany
[141] Affiliated with an Institute Covered by a Cooperation Agreement with CERN, Geneva, Switzerland
[142] Affiliated with an International Laboratory Covered by a Cooperation Agreement with CERN, Geneva, Switzerland

[a] Also at: Max-Planck-Institut fur Physik, Munich, Germany
[b] Also at: Italian National Agency for New Technologies, Energy and Sustainable Economic Development (ENEA), Bologna, Italy
[c] Also at: Dipartimento DET del Politecnico di Torino, Turin, Italy
[d] Also at: Yildiz Technical University, Istanbul, Türkiye
[e] Also at: Department of Applied Physics, Aligarh Muslim University, Aligarh, India
[f] Also at: Institute of Theoretical Physics, University of Wroclaw, Wrocław, Poland

[g] Also at: An Institution Covered by a Cooperation Agreement with CERN, Geneva, Switzerland
[*] Deceased